Circulation Research

ORIGINAL RESEARCH

Reduction of Cardiac Fibrosis by Interference With YAP-Dependent Transactivation

Gloria Garoffolo, Manuel Casaburo, Francesco Amadeo, Massimo Salvi, Giacomo Bernava, Luca Piacentini, Isotta Chimenti, Germana Zaccagnini, Gesmi Milcovich, Estella Zuccolo, Marco Agrifoglio, Sara Ragazzini, Otgon Baasansuren, Claudia Cozzolino, Mattia Chiesa, Silvia Ferrari, Dario Carbonaro, Rosaria Santoro, Martina Manzoni, Loredana Casalis, Angela Raucci, Filippo Molinari, Lorenzo Menicanti, Francesca Pagano, Toshiro Ohashi, Fabio Martelli, Diana Massai, Gualtiero I. Colombo, Elisa Messina, Umberto Morbiducci, Maurizio Pesce

BACKGROUND: Conversion of cardiac stromal cells into myofibroblasts is typically associated with hypoxia conditions, metabolic insults, and/or inflammation, all of which are predisposing factors to cardiac fibrosis and heart failure. We hypothesized that this conversion could be also mediated by response of these cells to mechanical cues through activation of the Hippo transcriptional pathway. The objective of the present study was to assess the role of cellular/nuclear straining forces acting in myofibroblast differentiation of cardiac stromal cells under the control of YAP (yes-associated protein) transcription factor and to validate this finding using a pharmacological agent that interferes with the interactions of the YAP/TAZ (transcriptional coactivator with PDZ-binding motif) complex with their cognate transcription factors TEADs (TEA domain transcription factors), under high-strain and profibrotic stimulation.

METHODS: We employed high content imaging, 2-dimensional/3-dimensional culture, atomic force microscopy mapping, and molecular methods to prove the role of cell/nuclear straining in YAP-dependent fibrotic programming in a mouse model of ischemia-dependent cardiac fibrosis and in human-derived primitive cardiac stromal cells. We also tested treatment of cells with Verteporfin, a drug known to prevent the association of the YAP/TAZ complex with their cognate transcription factors TEADs.

RESULTS: Our experiments suggested that pharmacologically targeting the YAP-dependent pathway overrides the profibrotic activation of cardiac stromal cells by mechanical cues in vitro, and that this occurs even in the presence of profibrotic signaling mediated by TGF-β1 (transforming growth factor beta-1). In vivo administration of Verteporfin in mice with permanent cardiac ischemia reduced significantly fibrosis and morphometric remodeling but did not improve cardiac performance.

CONCLUSIONS: Our study indicates that preventing molecular translation of mechanical cues in cardiac stromal cells reduces the impact of cardiac maladaptive remodeling with a positive effect on fibrosis.

GRAPHIC ABSTRACT: A graphic abstract is available for this article.

Key Words: cell mechanics ■ fibrosis ■ heart failure ■ myofibroblasts ■ stromal cell ■ YAP transcription factor

Meet the First Author, see p 187

Maladaptive remodeling of the myocardium is one of the earliest hallmarks of heart failure. This is characterized by inflammation and a progressive fibrosis that leads to replacement of the parenchyma with a stiff, fibrotic, tissue.[1] In the adult healthy myocardium, the turnover of the ECM (extracellular matrix) is controlled by stromal interstitial cells, which can be mapped into several different phenotypes based on transcriptional and functional features.[2–4] Under conditions causing ventricular mechanical overload (eg, hypertension), in the presence of metabolic alterations such as hyperglycemia, injury such as hypoxia, or just depending

Correspondence to: Maurizio Pesce, PhD, Cardiovascular Tissue Engineering Research Unit; Centro Cardiologico Monzino, IRCCS, Via C. Parea, 4, I-20138, Milan, Italy. Email maurizio.pesce@ccfm.it

Supplemental Material is available at https://www.ahajournals.org/doi/suppl/10.1161/CIRCRESAHA.121.319373.
For Sources of Funding and Disclosures, see page 255.

Circulation Research is available at www.ahajournals.org/journal/res

Novelty and Significance

What Is Known?

- Sensing of mechanical cues is crucial for acquisition of pathological phenotypes in cardiovascular tissues remodeling.
- The identity and the function of mechanically regulated transcriptional activators in cardiac pathology has been clarified mainly with genetic studies.
- The transcription factor YAP (yes-associated protein) is involved in the fibrotic evolution of cardiac stromal cells.

What New Information Does This Article Contribute?

- YAP-dependent transactivation is regulated by strain/compression forces in 2-dimensional/3-dimensional in vitro models and in a mouse model of ischemic heart failure.
- Pharmacological interference with the nuclear function of YAP overrides TGF-β1 (transforming growth factor beta-1)-dependent profibrotic programming in vitro.
- The use of a YAP targeting molecule in vivo reduces the extent of cardiac fibrosis.

Emerging evidence suggests that mechanical signaling is crucial for acquisition of pathological phenotypes during cardiovascular tissue remodeling. While the identity and the function of mechanically regulated transcriptional activators in cardiac pathology has been clarified mainly with genetic studies, a direct connection between cell mechanics and progression of ischemia-dependent fibrosis was heretofore missing. In the present contribution, we show that nuclear translocation of the YAP transcription factor occurs by exposing cardiac fibroblasts to incremental strain/compression forces either in vitro or in vivo. We also provide evidences that pharmacological interference with the nuclear function of YAP is sufficient to override TGF-β1-dependent profibrotic programming in vitro, and to reduce the extent of cardiac fibrosis in vivo. Our results open the way to 'mechano-therapeutics' of the fibrotic heart.

Nonstandard Abbreviations and Acronyms

ECM	extracellular matrix
MI	myocardial infarction
TAZ	transcriptional coactivator with PDZ-binding motif
TEAD	TEA domain transcription factor
TGF-β1	transforming growth factor beta-1
VTP	verteporfin
YAP	yes-associated protein

on the aging process, resident unactivated stromal cells evolve into profibrotic cells, the so-called myofibroblasts (Myo-Fbs) that contribute to inflammation, altered ECM accumulation, and myocardial stiffening.[5–10]

The term mechanosensation refers to the ability of the cells to sense the physical characteristics of the surrounding environment through the activation of intracellular signaling cascades elicited by mechanical cues.[11] The Hippo signaling pathway, an essential component of the machinery translating cell mechanical responses into discrete transcriptional activation is well contextualized in cancer biology as a *primus movens* in cancer stem cells determination, metastatic activity, drug resistance, and cell plasticity.[12] A direct connection between static/dynamic mechanical cues and transcriptional activation of downstream targets has been established with the finding that cytoskeletal tensioning resulting from cellular adhesion to extracellular components with specific geometric arrangement and viscoelastic properties[13] translates into reversible nuclear shuttling of the main Hippo transcriptional component, the YAP (Yes-associated protein)/TAZ (transcriptional coactivator with PDZ-binding motif) complex.[14–16] In addition to promoting shuttling from the cytoplasm to the nucleus of the YAP/TAZ complex by inhibiting the Hippo kinase pathway, the acto-myosin cytoskeleton also directly forces YAP/TAZ into the nucleus by physically deforming the nuclear lamina and opening the nuclear pores.[17] The relevance of the Hippo signaling for cardiac biology has emerged from studies highlighting the role of YAP in neonatal myocytes proliferation and cardiac regeneration.[18–22] Moreover, specific deletion of upstream components of the Hippo pathway Lats1/2 in cardiac fibroblasts determines a permanent activation into Myo-Fbs,[23,24] strongly suggesting implication of the YAP/TAZ complex in homeostatic control of cardiac matrix, and a specific function in myocardial remodeling after injury. In keeping with these evidences, elevated levels of nuclear YAP have been found in infarcted hearts in mice,[25] and blockade of YAP/TAZ complex activity with VTP (verteporfin), a drug that interferes with the binding of the complex to TEADs (TEA domain transcription factors) DNA-binding proteins, attenuates injury-dependent cardiac fibrosis.[26,27] The link between the abnormal distribution of the straining forces in the infarcted heart and activation of the YAP-dependent transcriptional activation is, however, not clear. It is also not clear whether human myocardial stromal cells respond directly to strain forces

with activation of YAP-dependent profibrotic signaling. In the present study, we provide evidences that the straining forces acting upon remodeling of the myocardial matrix after infarction activate the Hippo transcriptional pathways through a mechanism determining nuclear straining and preferential cellular polarization in the infarct scar. We also show that cardiac stromal cells (cSt-Cs) activate a profibrotic pathway in response to sensing of tissue compliance and geometry, thus linking YAP nuclear translocation to the force-dependent matrix remodeling process occurring during the cardiac healing after infarction. This process can be reverted by treatment with VTP even under high-strain conditions and in the presence of TGF-β1 (transforming growth factor beta-1), a key paracrine stimulator of cardiac fibrosis.[28] These findings were obtained in mice carrying permanent ligature of the left anterior descending coronary, in which treatment with VTP reduced fibrosis at short- and long-term after ischemia.

METHODS

Data Availability

Data, methods and materials used in the present investigation are available upon request to the corresponding author.

The RNA-seq data have been deposited at the NCBI Gene Expression Omnibus (GEO) repository and will be freely accessible at https://www.ncbi.nlm.nih.gov/geo/query/acc.cgi?acc=GSE203358. The code for RNA-seq analysis is freely available at https://github.com/BioinfoMonzino/Garoffolo_etal_CircRes_2022.

Ethics

Experimental investigations involving human-derived cells and tissues were approved by the local ethical committee at Centro Cardiologico Monzino, IRCCS (approval date: 19 May 2012 and subsequent renewal on 16 May 2016) and Policlinico San Donato, IRCCS (protocol 2438, 27/01/2009 and CE 85/int/2016 9/6/2016). Collection of material and experiments were performed in compliance with the Declaration of Helsinki. Patients were required to sign an informed consent to donate small fragments of cardiac tissue (right atrial appendage), during coronary bypass grafting or aortic valve substitution interventions. Experiments in mice were conducted in keeping with the guidelines from Directive 2010/63/EU of the European Parliament on the protection of animals used for scientific purposes, and in accordance with experimental protocols approved by the University Committee on Animal Resources at the University of Milan (668-2015). The protocol of VTP in vivo administration in mice with permanent myocardial infarction (MI) was approved by the Italian Ministry of Health (Authorization number 861-2021) and were executed in an authorized facility.

Mouse Model of MI

A mouse model of permanent ligature of the left anterior descending coronary artery was employed to create a MI. Mice were sacrificed at short (3 days), intermediate (7 days), and long (4 weeks) follow-up times, after which hearts were prepared for histological analysis. The protocol of in vivo treatment of mice with VTP was performed by administrating VTP dissolved in corn oil at a concentration of 50 mg/kg every third day. Monitoring of the treatment effect was performed by echocardiography at specific steps during the observation period. At the end of the treatment, the hearts were harvested and processed for histology. For further information on animal procedures, see the extended methods available in the Supplemental Material.

Microfabrication Methods

For the manufacturing of the controlled stiffness gels with polyacrylamide (PAA), we used a protocol that was previously employed by us.[29] For investigating the traction forces generated by single cells, the micropillar method was adopted.[30,31] The manufacturing of the micropatterned substrate of poly(dimethylsiloxane) (PDMS, Sylgard 184, Dow Corning), a dedicated silicon mold with a negative pattern of the micropillar arrays was designed using the software Solidworks (Dassault Systemes, Vélizy-Villacoublay, France). Further details about design and fabrication of the microfabricated structures are provided in the extended methods available in the Supplemental Material.

Primary Cell Culture, Human Tissue Harvesting, and Main Immunofluorescence Methods

Primary human cardiac stromal cells were derived from "cardiospheres" as previously described.[32,33] Briefly, cellular outgrowths of small myocardial explants were subcultured to obtain cardiospheres and cardiospheres-derived primitive cSt-Cs. Cardiospheres and cSt-Cs were used for immunofluorescence staining and high content image analysis using CARE, an algorithm originally developed by us to analyze microscopic images.[34] Controls of immunofluorescence/histochemistry included samples stained with preimmune antibodies/sera and also secondary antibody-only stained samples to determine the background level. For exhaustive information on cell culture methods and cell analyses, see the extended methods. For the observations on human myocardium, left ventricle cardiac biopsies were harvested from patients affected by dilated hypokinetic ischemic cardiomyopathy undergoing surgical ventricular reconstruction procedure. Formalin-fixed paraffin-embedded consecutive serial sections (1 µm thickness) of the border zone samples (peri-infarct area) were dewaxed and hydrated through graded decrease alcohol series and stained for histological analysis. Hematoxylin/Eosin staining (Mayer's Hematoxylin/Eosin; Bio Optica, Milan, Italy) and Masson Trichrome staining (Masson trichrome with aniline blue Bio-Optica) were carried out using standard protocols. The microscopic images contained in the figures are those that best represent the observed phenotypes.

Atomic Force Microscopy

Force spectroscopy measurements were performed with a commercial atomic force microscope mounted on an inverted microscope using a borosilicate glass microsphere of about 18 µm in diameter manually glued at the end of the cantilever.

Cell rigidity was evaluated in 30 randomly chosen cells for each condition, acquiring 3 force spectroscopy curves in the center of each cell nuclei. Further details are provided in the Supplemental Material.

Molecular Methods

For Western blotting analyses, cells were lysed in standard sample buffer and run (30 µg) into 4% to 12% gradient SDS polyacrylamide gels. Proteins were transferred onto nitrocellulose membranes followed by incubation with the indicated primary and secondary antibodies (see Major Resource Table). For RNA-sequencing analysis, total RNA was extracted from 6 independent cSt-Cs cultured ±TGF-β ±VTP using TRIzol. After quality checking and quantification, the Poly(A)$^+$ RNA was enriched and then processed for RNAseq. Differential gene expression analysis was performed using the R software. Validation was performed in independent RNA samples of cSt-Cs by RT-qPCR. Indications about the primers sequences and reagents are provided in the Major Resource Table. The effects of TGF-β1±VTP on cSt-Cs contraction were determined using a cell contraction assay kit (Cell Biolabs), as per the Manufacturer's instructions. Collagen plug areas were measured using ImageJ software. Soluble collagen release was quantified using Sircol colorimetric assay (Biocolor) on conditioned medium of cSt-Cs. A full description of the methods employed in molecular analyses is provided in the online supplementary material.

Statistical Analyses

Data were graphed and analyzed using the Prism Graph Pad statistical software. Normality tests on normal/log-normal distributions were run using the Shapiro-Wilk methods fixing α=0.01. The number of replicates, the *P*, and the type of tests that were used for statistical comparisons are specified by the dots/numbers over the histograms in the figures and the figure legends, respectively.

RESULTS

Orientation- and Cell Strain-Dependent Activation of YAP in the Infarct Scar

To assess the activation of the YAP-dependent transcriptional pathway in the context of the late myocardial remodeling occurring after ischemia, we performed immunohistochemistry on hearts of mice with permanent ligature of the left coronary artery at early (3 days) and late (4 weeks) follow-up.[35] Figure 1A shows the results of YAP immunolocalization in transversal sections of the infarcted heart at 3 days post-MI. Cells with the morphology of monocytes/macrophages invading the infarct area exhibited, in line with the literature,[36] high levels of the protein in the nucleus. Cells showing nuclear-localized YAP included also putative myofibroblasts and cardiomyocytes. In the remote zone, a reduced number of cells were positive for YAP (independently of nuclear/cytoplasmic localization), suggesting an ischemia- and or inflammatory-dependent activation of the pathway in the infarcted region. At 4 weeks after infarction, infarct scars with abundant collagen deposition were clearly visible (Figure 1B). In this fibrotic tissue, collagen bundles and cells with Myo-Fbs morphological characteristics were clearly recognizable with a preferential equatorial/circumferential orientation (see insets in the figure). Analysis of YAP expression in the fibrotic tissue by immunohistochemistry revealed cells with Fibroblasts (Fbs) morphology bearing high levels of YAP nuclear localization (YAP$^+$) or negative for expression of the transcription factor (YAP$^-$; Figure 1C). Examining the IHC images at high magnification, it came to our attention that YAP$^+$ cells were not evenly distributed in the collagen-rich matrix but exhibited a preferential nuclear orientation along the equatorial cutting plane of the left ventricle suggesting a relationship between nuclear translocation of the transcription factor and strain forces transmitted within the circumferentially arranged collagen fibers (Figure 1B).[37] To quantify this finding, we determined the nuclei orientation and deformation in these cells using CARE, an algorithm that we previously tailored to perform automatic segmentation of microscope images[34] (Figure 1C and 1D, Figure S1). We then correlated these values to the presence of nuclear YAP. Figure 1E contains the results of this analysis, showing a significantly higher nuclear deformation and a more frequent equatorial alignment of YAP$^+$ compared with YAP$^-$ cells. This suggests that strain forces, known to direct anisotropic collagen deposition in the forming scar,[37] are also involved in the activity of the YAP/TAZ transactivation pathway connected to nuclear deformation and equatorial alignment of cells with CFs morphological characteristics in the fibrotic areas.[17] These results were validated in myocardial tissue of patients with severe heart failure undergoing surgical ventriculoplasty. As shown in Figure 1F, the interstitial fibrosis, well evident in the tissue, was associated with presence of cells with YAP staining in the nucleus, suggesting activity of the pathway in cells of the fibrotic scar.

YAP Nuclear Translocation is Mechanically Regulated by Cytoskeleton Tensioning in Human Cardiac Stromal Cells and is Correlated to Expression of Fibrotic Markers

To prove that YAP nuclear translocation is mechanically connected to cytoskeleton tensioning in cells with the ability to differentiate into Myo-Fbs, we derived cardiac stromal cells from human primary explant cultures from human right atrial fragments,[32] selected through spontaneous spheroid growth (the so-called cardiosphere)[38] for a primitive mesenchymal phenotype. In line with the existing literature,[39] cardiosphere-derived cells exhibited a variety of mesenchymal markers including CD29, CD44, CD90, and CD105 but not endothelial markers CD31 and CD144 (Figure S2). We first employed 2D polyacrylamide gels (PAGs) with a discrete stiffness in the range of 17 to 58 kPa (Young's elastic

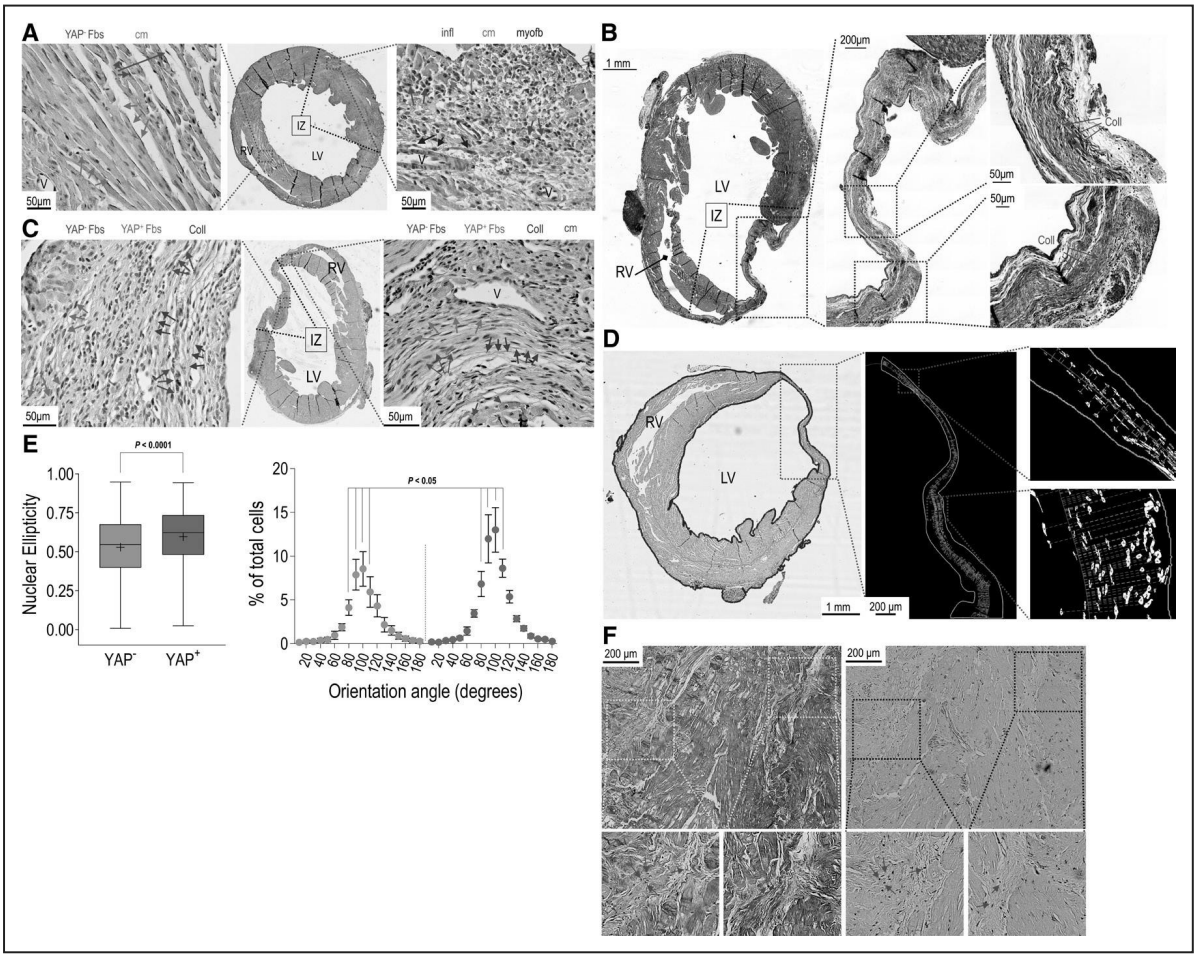

Figure 1. Activity of YAP (yes-associated protein)-dependent signaling is subjected to oriented nuclear straining and cellular alignment in the infarct scar.

A, Equatorial section of the infarcted heart showing the left and right ventricles (LV and RV, respectively) at a short follow-up time (3 days post-myocardial infarction [MI]) stained with anti-YAP antibodies. The higher magnification on the left side of the panel shows the presence of cardiomyocytes (cm) and fibroblasts (Fbs) characterized by low levels of nuclear YAP. A preferential localization of YAP$^+$ cells was observed in the infarct zone (IZ) magnified in the right side of the panel, which at this time point is not yet subjected to extensive remodeling, but is affected by a high degree of inflammation. At this stage, YAP nuclear signal was detected in inflammatory infiltrate cells (infl), in some myofibroblasts (Myo-Fbs) and cardiomyocytes (cm). **B**, Masson trichrome staining of a terminal stage (4 weeks post-MI) cardiac remodeling, characterized by the presence of a collagen-rich scar extending from the wall of the RV to a wide portion of the LV. On the left side of the panel, it is represented the whole equatorial section of the heart to show the totality of the remodeling process. In the center and the right of the panel are represented two consecutive magnifications of the areas of the infarct zone (IZ) encircled by the blue dotted squares, to show the orientation of the collagen (Coll) bundles along a preferential equatorial plane (red arrows). Note the presence of numerous fibroblasts exhibiting a similar orientation. **C**, YAP immunohistochemical labeling of the same heart cut with the same equatorial orientation shown in **B**. The magnification of the two areas encircled by the red dotted squares show the presence of collagen bundles (Coll; blue arrows) and of fibroblast-resembling cells characterized by presence of YAP in the nucleus (YAP$^+$, green arrows) or absence of the transcription factor (YAP$^-$), indicated by red arrows. Note in both panels that cells with YAP$^+$ nuclei appeared in both areas to show a higher nuclear aspect ratio (ellipticity). **D**, Virtual reconstruction of the nuclei orientation in the infarct scar as detected by CARE. On the left side of the panel, it is represented the actual image of an equatorial section of LV and RV of a heart with an end-stage remodeled infarct zone (red dotted square), with an indication of the profiles of the external cardiac wall and the internal LV wall (both indicated by blue lines) and the midline of the wall (green line). The panel in the center shows the margins of the scar (green lines) defined by the two concentric lines contouring the collagen-rich region in the scar, and the scar centerline (red). The orientation of each cell nucleus was measured by determining the tilting of the major nuclear axis with respect to the line intersecting perpendicularly the scar midline in manually selected zones with a clearly visible fibrotic appearance in the scars (green boundaries in the right; see also Figure S1). **E**, Comparison of nuclear ellipticity and orientation as computed by CARE for YAP$^+$ and YAP$^-$ nuclei in the terminally remodeled infarct of 3 mice with a 4-week post-MI follow-up. The box plot on the left represents the min-max distribution, the median and the mean (+) of the nuclear aspect ratio in YAP$^-$ (blue) and YAP$^+$ (brown) nuclei. Data were analyzed by Mann-Whitney *t* test (n=3329 YAP$^-$ and n=4559 YAP$^+$ nuclei, respectively). The two distributions on the right side of the panel show the percentage of the cells with nuclei with an orientation (θ) ±10° in a $0° < \theta < 180°$ range with respect to the perpendicular direction to the scar center line (see **E** and Figure S1). Data in the two distributions are indicated as percentage (±SE) of YAP$^-$ (blue) or YAP$^+$ (brown) nuclei of the total amount of computable nuclei in the scar of 3 mice within the 18 resulting ±10° orientation categories. As shown, the percentage of YAP$^+$ nuclei with an orientation ±10° within the $70° < \theta < 110°$ range were significantly higher than that of YAP$^-$ nuclei. Data were compared by unpaired multiple *t* test analysis. **F**, Low and high magnification of representative sections of human myocardium from patients with dilated hypokinetic ischemic cardiomyopathy stained with Masson's trichrome and YAP IHC. In the lower insets it is evident the presence of numerous fibroblasts with YAP$^+$ nuclei populating the collagen scar.

modulus, detected by atomic force microscope)[29] and, as a reference, glass surfaces to promote cell attachment onto fibronectin. Results of cytoskeleton staining by phalloidin-TRITC revealed a decrease in stress fibers polymerization and consequent changes in cellular forms factors (area and circularity) onto softer gels (Figure 2A). To unravel the role of environmental mechanics on YAP-dependent nuclear signaling,[15,16] we performed YAP staining of the cells plated onto PAGs followed by quantitative evaluation of the cells with nuclear-localized YAP (nYAP$^+$ cells) and of the cytoplasmic/nuclear YAP signal ratio (Figure 2B; Figure S3). As expected,[16,40] results showed a stiffness-dependent trend of YAP to be confined in the nucleus, and this was also directly connected to cell proliferation, as detected by labeling cells with Ki-67 antibody (Figure 2C).

Since the changes in proliferation and YAP nuclear/cytoplasm ratio observed in cells plated onto PAGs with controlled stiffness could be due to variations in cytoskeleton polymerization/tensioning,[17] we explored the possibility that cSt-Cs in a 3D structure could sense geometric or positional information translating into discrete YAP nuclear translocation and activation of profibrotic signaling. To validate this hypothesis, we analyzed the distribution of YAP localization inside the cardiospheres. These structures have been in fact described as 3-dimensional models of cardiac niches with undifferentiated cells located in the core of the sphere and more differentiated cells with mesenchymal characteristics located in the external shell.[32,41,42] Figure 3A and 3B show, respectively, the structure of the cardiospheres and the localization of YAP protein and Ki67 proliferation marker in the 3D structures. By employing CARE[34] to analyze these structures in high-resolution images serially acquired along the vertical axis of the spheroid cell clusters (*z*-stack), we were able to clearly distinguish in the 3D volume an external shell of the cardiospheres, defined as the outer volume encompassing one-third of the radius of the spheroids, where cells with intranuclear YAP and Ki67 localization were preferentially localized, and an inner core where YAP was mainly cytoplasmic and Ki67 signal was absent (Figure 3A; Figure S4). As a first control in this experiment, we used immunostaining with antibodies specific for GATA-4, a cardiac-specific transcription factor that is not known to

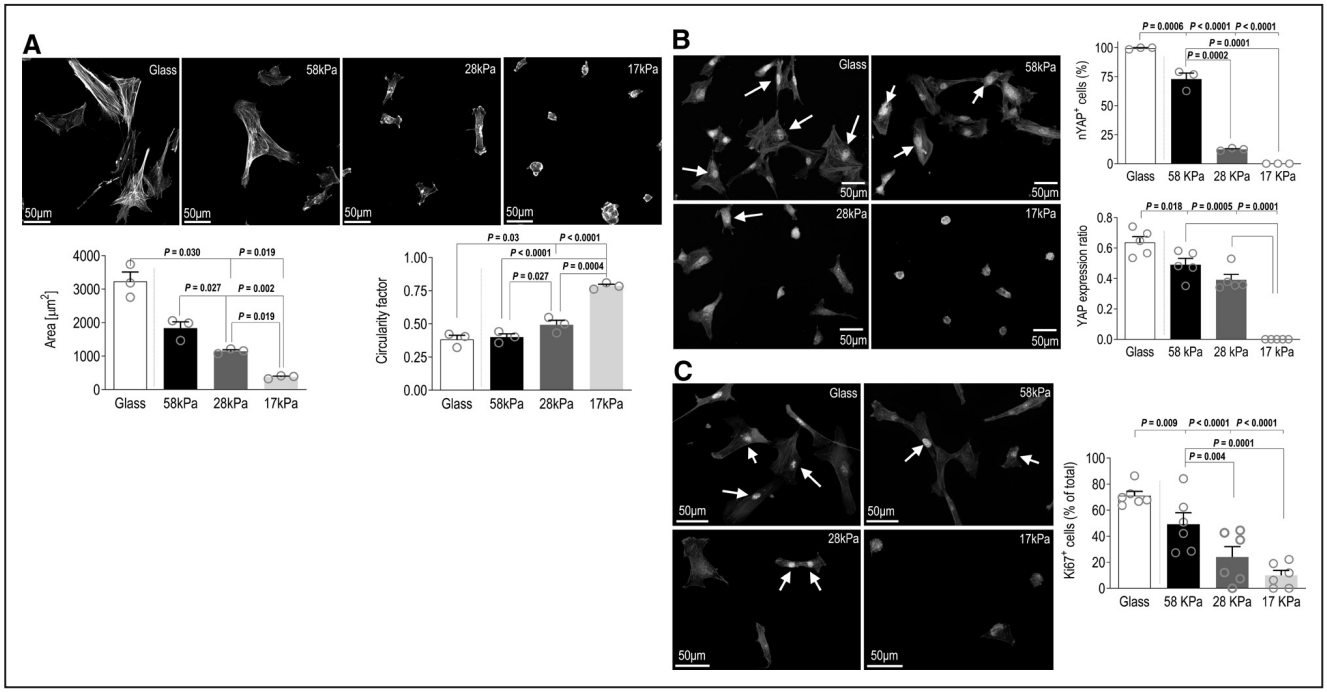

Figure 2. Strain-dependent activation of YAP (yes-associated protein) transcriptional pathway in human cSt-Cs.
A, Geometric features (cell spreading area; circularity) of human cSt-Cs are subjected to stiffness-dependent control. Cells were plated onto glass and onto a series of polyacrylamide gels with controlled stiffness ranging from 58 to 17 kPa (Young's modulus)[29] and were photographed to derive geometric information. The pictures show the staining of the nuclei (blue) and the F-Actin cytoskeleton by Phalloidin-TRITC (white color). The two graphs include areas (µm^2) and circularity factor from each of the indicated number of experimental replicates performed with cSt-Cs lines from different donors. **B**, The expression of YAP (green fluorescence) was visualized by IF along with the nuclear and F-Actin staining by DAPI (blue) and phalloidin-TRITC (red), respectively. The percentage of cells with nuclear-localized YAP (arrows) and the $YAP_{NUCL/CYTO}$ expression ratio were determined using ImageJ and CARE,[34] respectively (see also Figure S3). Graphs were derived with data obtained in at least 10 cells from each of the indicated number of experimental replicates performed with cell lines from different donors. **C**, Cells plated onto glass and PAGs with differential stiffness were labeled with Ki-67 proliferation marker (green, arrows) along with F-Actin (red) and nuclear (blue) staining. The graph shows the quantification of the results and indicates the statistical significance in the comparison between experimental groups. In all graphs in the panels, the *P* of the statistical comparisons between the cells plated onto glass vs PAGs with the different stiffness, or between cells plated on the differential stiffness PAGs are calculated by 1-way pairwise Anova with Dunnet and Tukey post hoc tests, respectively.

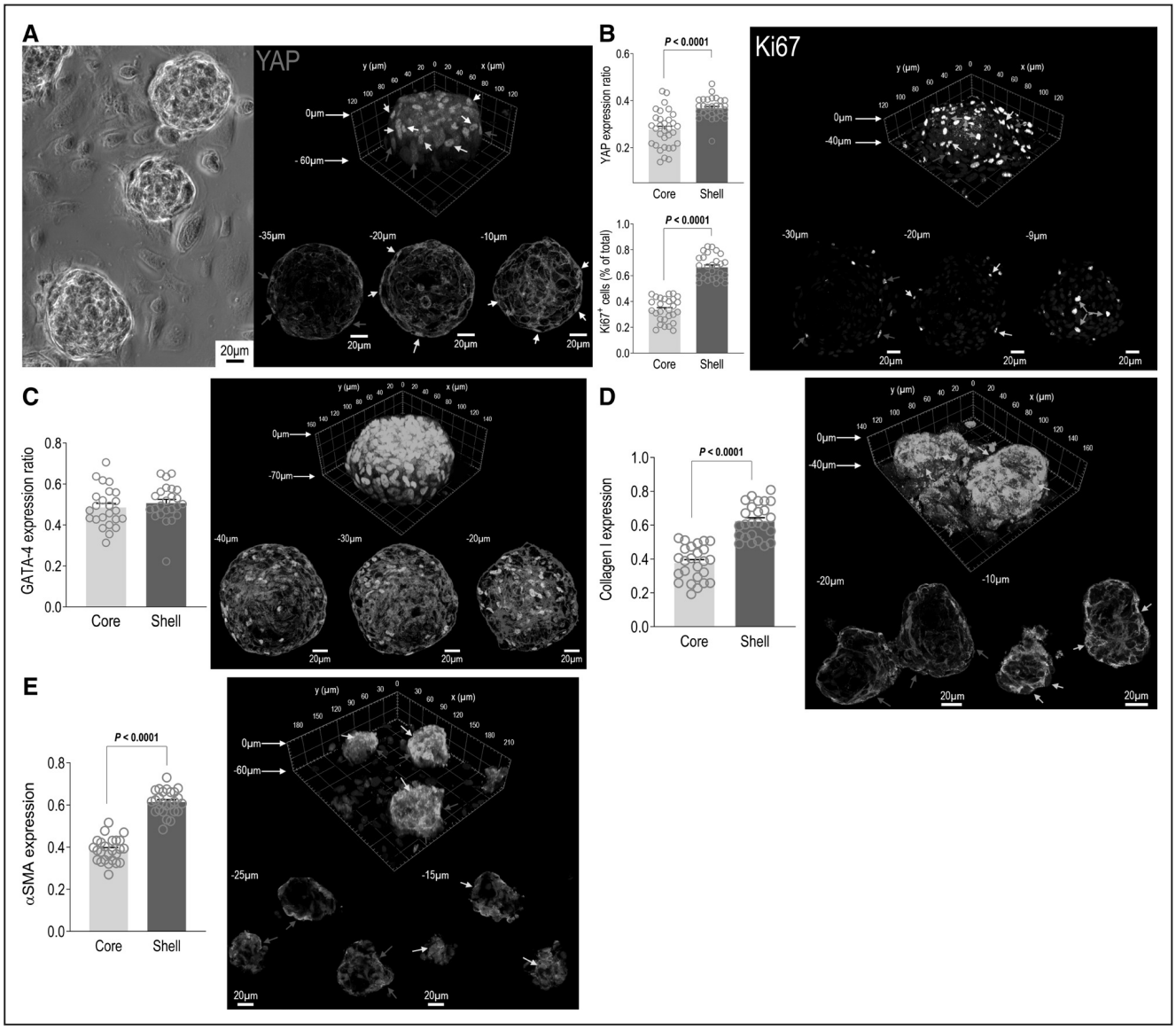

Figure 3. Topological cues support an asymmetrical distribution of cells with high $YAP_{NUCL/CYTO}$ expression ratio and proliferation/fibrotic markers in a 3-dimensional context.

A, Phase contrast view of primary cardiospheres derived from human myocardial tissue (left) and confocal image of a cardiosphere whole mount-stained with YAP (yes-associated protein)-specific antibody (green, right), F-actin (red), and nuclei. The image on the right shows, on the top, the 3D projection of the cardiosphere and the *x*, *y*, *z* dimensions (μm) as detected by high-resolution confocal imaging. The 3 images on the bottom show 3 discrete *x*, *y* equatorial images of the internal view of the same cardiosphere at the indicated distances (−35, −20, and −10μm) from the top of the sphere (set at 0 μm) along the *z* axis. In these images, it is evident the asymmetrical distribution of cells with YAP nuclear signal in proximity of the surface of the cardiosphere compared with its core. The arrows in different colors show examples of nuclei exhibiting a high content of nuclear YAP in the 3 equatorial images, also indicated with the same color code in the 3D projection on the top. **B**, On the right side of the panel, it is represented a confocal imaging 3D projection (top) and 3 *x*, *y* equatorial views (bottom) of a cardiosphere stained with Ki-67 antibody (white fluorescence) and nuclei (blue fluorescence) as described for **A**. The two graphs on the left represent, respectively, the $YAP_{NUCL/CYTO}$ expression ratio (top) and the percentage of the cells expressing Ki67 (bottom) as computed by CARE algorithm. **C**, The whole mount IF of GATA-4, a cardiac specific transcription factor, which is not known to be mechanically regulated, did not show differences in the nuclear/cytoplasm expression ratio between the shell and the core of the cardiospheres at any of the equatorial *x*, *y* projections. Data computation by CARE confirmed no statistically significant differences in the distribution of the ratios in the two compartments. **D** and **E**, Whole mount IF staining of cardiospheres with Collagen-I and αSMA antibodies, respectively, visualized as in **B** and **C**. As shown by the images and the *x*, *y* projections, these markers tended to be more expressed at the periphery and not in the center of the cardiospheres. Data computation with CARE performed on the fluorescence distribution in the shell vs. the core of the spheres showed a clear asymmetry, similar to that found for YAP. In all graphs, the *P* of statistical comparison by paired Student *t* test is shown. The number of cardiospheres (obtained from 4 independent tissue donors) introduced in the analyses are represented by the orange circles overlapped to the bars.

be mechanically regulated and, indeed, showed no preferential nuclear localization neither in the shell, nor in the core of the cardiospheres (Figure 3C; Figure S4). Second, given that the asymmetrical distribution may simply reflect possible metabolic stress of the cells in the core, due to limited distribution of nutrients and oxygen, we cultured

cSt-Cs in hypoxia, low glucose, and low serum conditions, and various combinations thereof. As shown in Figure S5, none of these conditions affected the YAP nuclear distribution in the cells, suggesting that asymmetrical YAP nuclear localization results from a differential response of the cells to compression forces deriving from topological cues. Finally, since YAP nuclear translocation is directly connected to cell mechanics-controlled proliferation and profibrotic activation,[43] we assessed the distribution of Ki67 and markers typically expressed in profibrotic cells in the heart (Collagen I and αSMA) in the cardiospheres. Results showed an overlapping between the regions of the cardiospheres where nuclear YAP, Ki67, and fibrotic markers were more frequently detected (Figure 3B, 3D, and 3E), suggesting a cause relationship between topological activation of YAP signaling and differentiation of cSt-Cs in profibrotic cells.

To establish a direct relationship between YAP localization and transmission of forces from the cytoskeleton to the nucleus, we investigated the nuclear ellipticity of cSt-Cs plated on 2D gels with differential stiffness and, in parallel, in the 3D cardiospheres volume. As shown in Figure 4A and 4B, there were significantly more round nuclear shapes in cells plated onto gels with low stiffness and in the core of the cardiospheres compared with gels with higher stiffness and the outer cardiospheres layer. We then directly interfered with the polymerization of stress fibers by treating cSt-Cs plated onto glass (stiffness in the MPa range) with Blebbistatin (BB) and Y27632.[44,45] Although these 2 compounds inhibit cytoskeleton tensioning with different mechanisms, both determined a completely reversible effects on stress fibers generation and nuclear YAP localization (Figure 4C and 4D). To assess whether nuclear straining by cytoskeleton tensioning is directly associated with modifications in nuclear geometry and mechanics, we used confocal imaging and atomic force microscope. Results of these analyses showed that both inhibitors reversibly increased the dimension along the *z*-axis of the nuclei of cSt-Cs, and determined a relaxation of their chromatin as detected by a decrease in nuclear stiffness (Figure 4E). Finally, to contextualize the results in the framework of the YAP-dependent transactivation, we analyzed the expression of 3 YAP canonical targets (*CTGF*, *CYR61*, *ANKRD1*) in cells treated with BB or Y27632 using RT-qPCR (Figure 4F). This experiment showed a completely reversible reduction in the expression level of the 3 genes versus controls. This establishes a connection between the expression of profibrotic genes and strain-dependent YAP transcriptional signaling in human cSt-Cs.

Override of the Profibrotic Mechanical Programming of Human cSt-Cs by Verteporfin

Results showing the reversible changes in nuclear shape and relaxation in cells treated with Actin cytoskeleton inhibitors indicated a possible way to interfere with YAP signaling and, thus, reverse the cSt-Cs profibrotic activation controlled by cell and nuclear mechanics. On the other hand, these inhibitors are quite unspecific and display an elevated cytotoxicity in vivo, thereby calling for more specific pharmacological inhibitors of the YAP nuclear functions. A more specific inhibitor was found in the VTP molecule, a drug with antifibrotic properties,[46,47] recently found to inhibit cardiac remodeling in mice.[26,48]

In the first series of experiments, cSt-Cs were treated with VTP under the maximal strain condition (culture onto glass) and then assayed for the expression of YAP target genes and genes involved in cardiac fibrosis.[26] To exclude that VTP has toxic effects on cells, we performed live/dead staining of cells treated with increasing amounts (1–10 μmol/L) of the drug for 5 hours, followed by a 48 hours observation period (Figure S6). Having excluded toxic effect of VTP, we then analyzed its biological effects. Figure 5A shows that a 5 hours treatment with the drug did not modify the cellular shape and did not affect YAP nuclear localization. By contrast, RT-qPCR experiments clearly showed a reduction in the expression of *CTGF*, *CYR61,* and *ANKRD1*, as well as of *Coll1A1*, *CollA3,* and *Thy-1*, which are typical markers of cells with a fibrotic phenotype.[49]

We then analyzed the effects of a more chronical treatment with VTP (3 days) in the context of the signaling induced by TGF-β1, one of the most potent inducers of cardiac fibrosis.[50] In these experiments, we co-treated cSt-Cs with TGF-β1 (±VTP) and assessed the expression of fibrotic genes after 72 hours using an RNA sequencing approach. Following data processing and raw count filtering criteria, we identified 17781 expressed genes, which included 13112 protein coding genes (74%), 2823 pseudogenes (16%), 1770 long noncoding genes (10%), and a small fraction of small noncoding genes (<<1%) (Gene ID details in supplementary bioinformatics data –a). Paired-sample analysis adjusted for confounding "latent" variables allowed reducing the effects of heterogeneity among subjects, thus unveiling specific changes between each treatment versus CTRL. We report the overall results and statistics for each statistical model in the supplementary material, and summarize the main findings in Figure S7A and S7B with a representation of the differentially expressed genes in the comparisons of the treated cells versus control cells, or in the VTP+TGF-β1 versus TGF-β1 condition. In brief, we found a substantial number of differentially expressed (DE) genes by comparing the mRNAs of VTP-treated cells (±TGF-β1) versus CTRL and to a lesser extend also for the treatment with TGFβ alone. On the other hand, 103 out of the 196 genes up-regulated by TGFβ were downregulated by co-treatment with VTP, indicating that VTP has a down-regulatory effect on genes induced by the profibrotic cytokine (Figure S8). This evidence was supported by the results

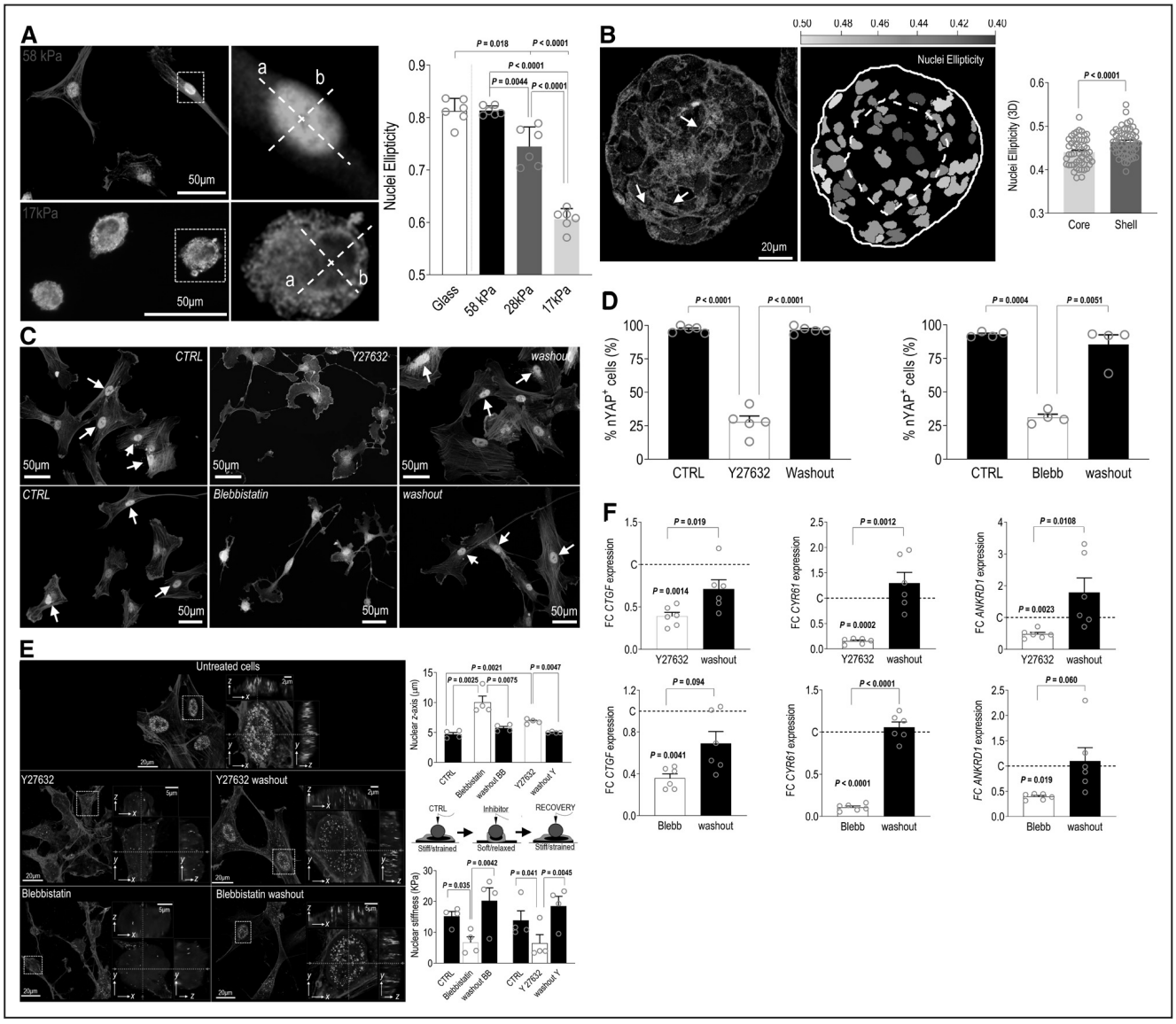

Figure 4. Nuclear geometry and tensioning regulates activity of YAP (yes-associated protein) transcriptional pathway in human cSt-Cs.

A, Comparison between the shape of the cSt-Cs when in contact with hard (58kPa) and soft (17kPa) substrates. The low magnifications on the left show the cellular shape along with the YAP labeling (green); the magnifications of the areas encircled with the dotted squares on the right show the major (a) and the minor (b) axes, used to calculate the aspect ratio (Ellipticity) of the nuclei. Note that in cells in contact with the soft substrate, YAP fluorescence was almost localized almost entirely in the cytoplasm, while in cells adhering onto the stiff substrate it was almost entirely into the nucleus (see also Figure 2 for quantifications). The graph on the right shows the quantification of nuclear ellipticity in cSt-Cs plated onto the whole series of PAGs (plus glass as a control). The *P* of the statistical comparison of the nuclear aspect ratio in cells the cells plated onto glass *vs.* PAGs with the different stiffness, or between cells plated on the differential stiffness PAGs are indicated. These values were calculated by 1-way pairwise Anova with Dunnet and Tukey post hoc tests, respectively. **B**, Calculation of the nuclear aspect ratio in the cardiospheres with CARE. The two images show, respectively, the equatorial section of a cardiosphere labeled as in Figure 3, with YAP antibody (green), for F-Actin (red) and nuclei. Arrows indicate filamentous Actin labeling, showing putative stress fibers. The image on the right is the virtualization of the nuclei image in the left with an indication of the shell and the core of the sphere (see also Figure S4). This image contains a color-coded nuclear structural information according to a nuclear ellipticity scale comprised in this panel between 0.40 and 0.50. It is evident that the majority of the nuclei with higher aspect ratio were present in the shell of the sphere and that more round nuclei were abundant in the core. The graph on the right is a statistical comparison of the average nuclear ellipticity in the shell and the core in the indicated number of cardiospheres. The *P* of data statistical comparison by paired student's *t* test is indicated above the graph. **C**, Cellular effects of treating cSt-Cs with ROCK inhibitor Y27632 and Myosin II inhibitor Blebbistatin on substrate with maximal stiffness (glass). Cells are labeled with YAP antibody (green), F-Actin label (Phalloidin-TRITC, red) and nuclei (DAPI, blue). Before treatment (CTRL, left), cells exhibited a normal fibroblastoid/mesenchymal phenotype and nuclei with a high level of nuclear YAP (arrows). Treating them with both inhibitors (center panels in **C**) reduced the number of stress fibers and induced a change in cell shape, with a consistent reallocation of the YAP fluorescence in the cytoplasm. A re-tensioning of the stress fibers was observed with washout of both drugs (right panels), along with a return to normal level of YAP nuclear confinement (arrows). **D**, Quantification of YAP nuclear confinement. *P* of data statistical comparison by 1-way pairwise ANOVA with Tukey post hoc test are indicated above each graph. **E**, Nuclear geometry and compliance are affected by release of cytoskeleton tensioning. (*Continued*)

of unsupervised hierarchical clustering, which allowed us to distinguish between the diverse treatment conditions and, in particular, indicated a clear distinction in the transcriptional signature of cells treated with VTP (±TGF-β1) and those that were cultured without the drug (Figure 5B). We validated the transcriptional signature by performing single RT-qPCR assays with specific primers for *CTGF*, a profibrotic factor expressed under the direct control of YAP/TAZ/TEAD complex,[51] for the 2 collagen-encoding genes *ColA1*, *ColA3,* and for *Thy-1* and *ACTA2*, the genes encoding for CD90 and *αSMA*, two markers of cardiac Myo-Fbs.[49,52] In all cases, treatment of the cells with VTP reverted the upregulation of these genes even below the level exhibited in control cells (Figure 5B), again confirming a potent transcriptional inhibitory effect of VTP in human cSt-Cs. Since interference with YAP signaling may also result in an imbalance in the expression of the Hippo pathway, we investigated the relative expression of genes with a functional annotation in the pathway. As shown in Figure 5A and 5C a number of DE genes were up- or downregulated in VTP-treated (±TGF-β1) versus untreated cells (±TGF-β1). Among the upregulated genes, we noticed the expression of *DVL2*, that in analogy to DVL, is involved in balancing the YAP cytosol/nuclear ratio[53,54] and that of *AMOTL1*, a member of the Angiomotin proteins family, which has a specific inhibitory function of YAP activity by promoting phosphorylation via LATS proteins.[55] It was also remarkable that VTP treatment determined downregulation of the transcripts of *LATS1/2*, the transcripts encoding for the kinases of the Hippo pathway directly promoting YAP phosphorylation and functional activity,[56] of *TJP1*, encoding for a tight junction protein positively regulating the TAZ/TEAD function[57] and of *YAP* mRNAs itself. Together, these results suggest that treatment with VTP determines an imbalance in numerous checkpoints of the finely regulated mechanism tuning the activity of the YAP/TAZ transcriptional function. To substantiate the action of VTP on cSt-Cs with the attribution of specific biological functions, we performed a Gene Ontology (GO) enrichment analysis of the DE genes in the various treatments. As expected, this showed a majority of pathways that were downregulated with high significance in VTP-treated cells (±TGF-β1) connected with extracellular matrix organization, cell migration, inflammatory responses and cytokines production (Figure S9A and complete description of the pathways in supplementary bioinformatics data—b), consistent with a reduction of the inflammatory and matrix remodeling activity of cells treated with VTP. Finally, to contextualize the inhibitory effect of VTP in the framework of the TGF-β-dependent transcriptional signaling, we performed *cis*-regulatory sequence analysis on down-regulated genes by VTP, and identified binding motifs and tracks associated with TEAD 1/3/4 and SMAD4 transcription factors among the most significant. As shown in Figure S9B (see also supplementary bioinformatics data—c), the analysis identified groups of genes that are likely co-downregulated by VTP, due to connection of the YAP/TAZ complex with transcriptional mediators downstream of TGF-β1 (SMADs), through cooperation of TEADs.

VTP Inhibits Proliferation and Reduces Matrix Remodeling Activity of Human cSt-Cs

Since conversion of cardiac stromal cells into Myo-Fb is accompanied by transitioning into a rapid proliferation phase under the control of TGF-β1 signaling,[50] or even mechanical cues regulated by YAP,[15,43] we determined the percentage of cells exhibiting PCNA staining in cSt-Cs cultured with or without TGF-β1±VTP onto glass slides. Results evidenced a sharp increase in the percentage of proliferating cells in the presence of TGF-β1 (Figure 6A), blunted by VTP treatment. In a previous study, we established a method to assess cell strain-dependent Myo-Fb differentiation onto substrates with discrete stiffness, by determining the loading of αSMA onto the F-actin cytoskeleton as a measure of the ability of the cells to evolve toward a contractile phenotype.[29] Adopting this system, we found a clear effect of TGF-β1 treatment in increasing the number of the fluorescence peaks showing co-localization of F-Actin and αSMA onto stress fibers, using confocal imaging (Figure 6B), thus confirming promotion of a

Figure 4 Continued. The pictures on the left show the normal (*x*, *y*) microscopic view of glass-adhering cSt-Cs labeled with YAP antibody (green), F-Actin probe (red) and nuclear label (blue). The pictures on the right of each panel show the projection of the cells circled with a dotted square, along the *x*, *z* and the *y*, *z* axes, as detected by super-resolution confocal imaging. It is evident that treatment with inhibitors determined a relaxation of the nuclei along the *z* axis and that after washout of the cells, the re-tensioning of the stress fibers caused a return to a nuclear flattening condition (in keeping with YAP nuclear segregation). The effect of nuclear geometry on nuclear mechanical characteristics is shown in the panels on the right, where a quantification of the nuclear geometric changes along the *z*-axis by both treatment (and the treatments washouts) is shown, together with the physical 'softening' of the nucleus, as detected by AFM force imaging. In both graphs, the *P* values of data statistical comparison by 1-way pairwise ANOVA with Tukey post hoc test are indicated above each graph. **F**, Transcriptional readout of cytoskeleton inhibition consisted of downregulation of canonical YAP targets, as shown by RT-qPCR amplification of *CTGF*, *CYR61* and *ANKRD1* gene transcripts. Note that the expression level of these genes returned to baseline after drugs washout. Data are represented as fold changes (FC) in the expression of each gene in the indicated condition with respect to the expression level in untreated cells (indicated with a C corresponding to a level=1) calculated by the $2^{-\Delta\Delta Ct}$ method. Statistics was calculated on the corresponding ΔCt values. Above all graphs, the *P* of RT-qPCR Delta-CT data statistical comparison by 1-way pairwise ANOVA with Tukey post hoc test indicate the significance of differences in the expression of each tested gene in VTP-treated *vs.* control cells.

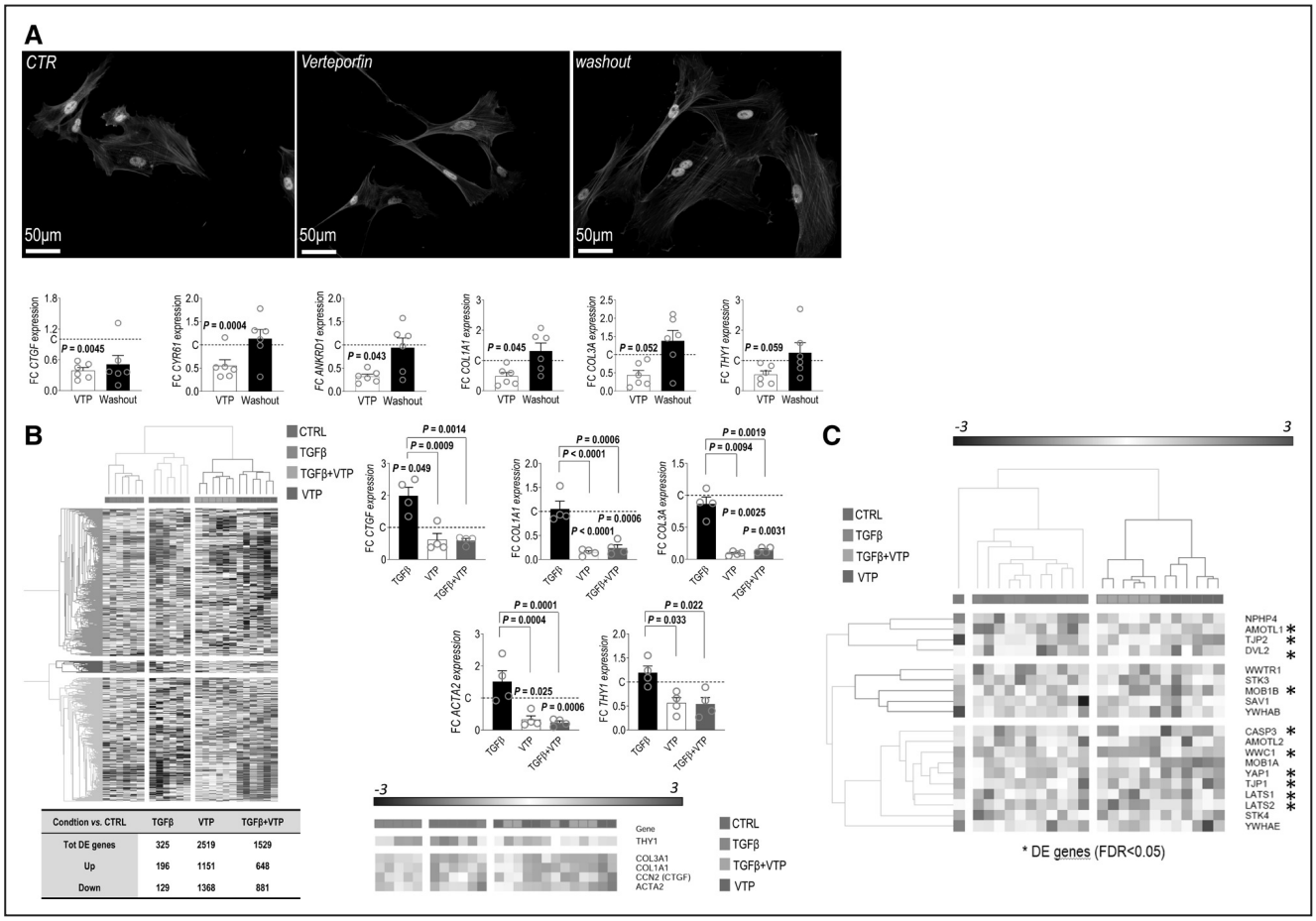

Condtion vs. CTRL	TGFβ	VTP	TGFβ+VTP
Tot DE genes	325	2519	1529
Up	196	1151	648
Down	129	1368	881

Figure 5. Global transcriptional effects of VTP (verteporfin).
A, cSt-Cs pulse-chased with VTP for 5 hours exhibited a partially reversible downregulation of YAP (yes-associated protein) target genes (*CTGF*, *CYR61*, *ANKRD1*) and profibrotic markers (*Col1A1*, *Col3A*, *Thy-1*). Transcriptional inhibition was not accompanied by cell morphological changes and YAP cytoplasm reallocation, as in experiments performed with cytoskeleton inhibitors Y27632 and blebbistatin (Figure 4). Data are represented as fold changes (FC) in the expression of each gene in the indicated conditions with respect to the expression level in untreated cells (indicated with a C corresponding to a level=1) calculated by the $2^{-\Delta\Delta Ct}$ method. Above all graphs, the *P* of RT-qPCR Delta-CT data statistical comparison by 1-way pairwise ANOVA with Tukey post hoc test indicate the significance of differences in the expression of each tested gene in VTP-treated vs control cells. **B**, Results of an RNAseq analysis of RNA samples extracted from control cSt-Cs, and cSt-Cs cultured ±TGF-β1 (±VTP) for 3 days. Hierarchical clustering was performed by Euclidean (sample) and 1-pearson correlation (genes) metric and average linkage method; gene expression levels are displayed as gradient colors from higher (dark red) to lower (dark blue). The heat map on the left shows the results of DE gene unsupervised clustering, exhibiting a nearly perfect clusterization of genes significantly regulated by the treatment with the drug. The table on the bottom indicates the number of the DE genes (adj. $P<0.05$ and $|log2FC|>0.58$) for each comparison between treatment vs CTRL. DE genes are also distinguished between those that are up- or down-regulated in each treatment vs CTRL. On the top right side of the panel, we report a representation of RT-qPCR analysis of 5 genes regulated by YAP whose modulation was consistent with the observed changes in the RNAseq profiling, in independent cellular replicates. In all panels, graphs were generated using the fold changes (FC) in the expression of each gene in the indicated conditions with respect to the expression level in untreated cells (indicated with a C corresponding to a level=1) calculated by the $2^{-\Delta\Delta Ct}$ method. Above all graphs, the *P* of RT-qPCR Delta-CT data statistical comparison by 1-way pairwise ANOVA with Tukey post hoc test indicate the significance of differences in the expression of each tested gene in VTP-treated *vs.* control cells or between treatments. The heat map on the bottom right indicates the variation in the expression of the same genes as represented in the general dataset of the DE mRNAs (bioinformatics Supplemental Material—a). **C**, Differential expression of genes with functional annotation in the Hippo pathway. With * are indicated differentially expressed genes (adj. $P<0.05$ and $|log2FC|>0.58$) found in at least one of the treatments vs CTRL comparison.

Myo-Fb phenotype. On the other hand, cells treated with VTP reduced, at least in part, the loading of αSMA onto the actin cytoskeleton, suggesting reversion of the Myo-Fb phenotype due to TGF-β1 treatment. To further validate the effect of VTP in reversing the Myo-Fb activation of cSt-Cs, we assessed the expression of αSMA using fluorescence quantification on confocal images and Western blotting, and by measuring the collagen secretion in the culture medium (Figure 6C). In line with the previous results, VTP reduced the expression of the Myo-Fb marker and the secretion of collagen even below the level of control cells. Finally, since the ability to remodel the extracellular matrix in the context of MI is a specific activity of Myo-Fbs, we measured the matrix compacting ability of the cSt-Cs treated with TGF-β1, and the reversal of this activity by VTP, using a collagen compaction in vitro assay. Results (Figure 6D) showed a clear contraction of

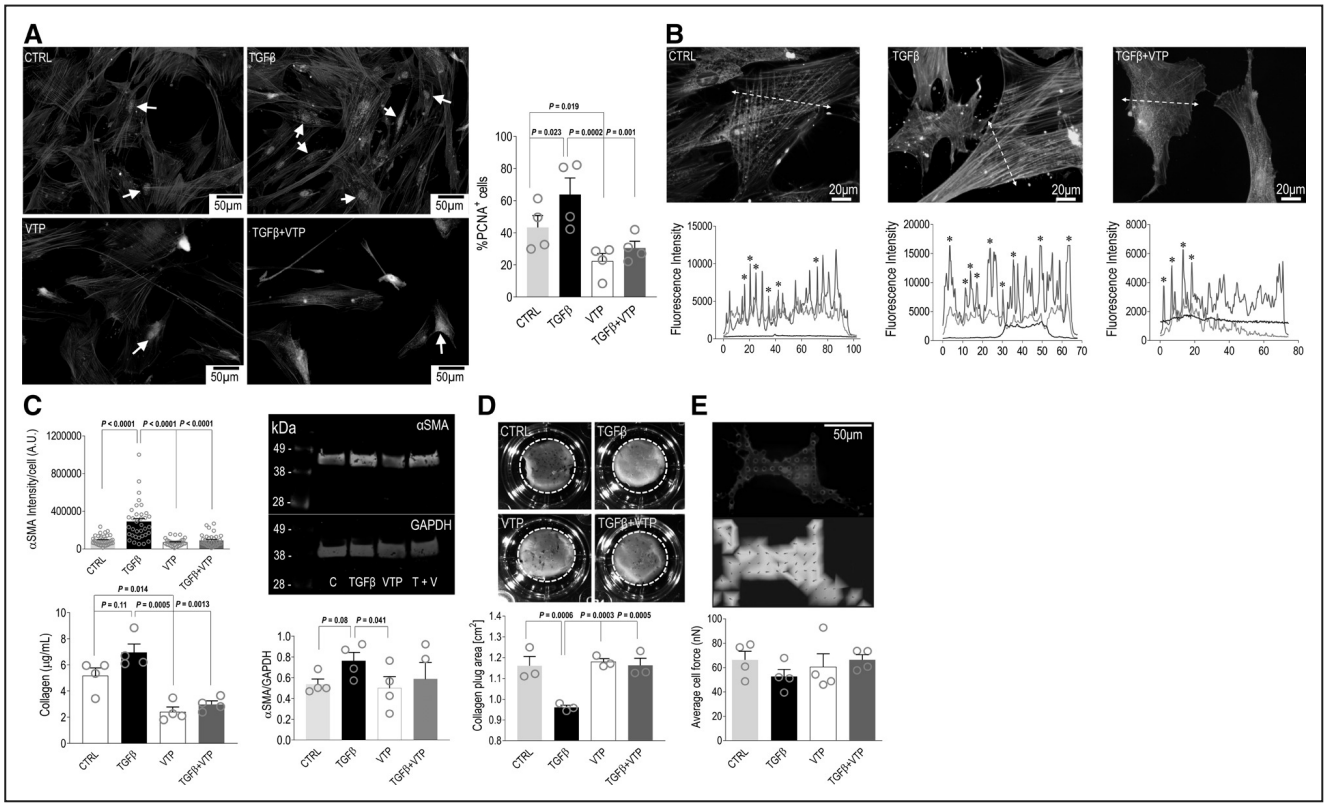

Figure 6. Biological effects of VTP (verteporfin) treatment in vitro.
A, Treatment with VTP reduces proliferation of human cSt-Cs, as assessed by IF staining with antibodies specific for PCNA (green fluorescence) and F-Actin (red fluorescence)/nuclear staining (blue staining). Note that the drug reduced the percentage of PCNA+ cells (arrows) below the control level even in the presence of TGF-β1 (transforming growth factor beta-1), supporting a strong reduction of cellular proliferation, a recurrent feature in conversion of primitive stromal cells into myo-FBs. Above the graph, the *P* indicate the results of data statistical comparison by 1-way pairwise ANOVA with Tukey post hoc test. **B**, cSt-Cs treated with VTP loose myo-FB characteristics promoted by TGF-β1, as detected by the unloading of αSMA (smooth muscle actin-alpha) from F-Actin cytoskeleton. The three images on the top show three cells labeled with F-Actin (red fluorescence) and nuclear staining (blue fluorescence) along with αSMA antibody (green fluorescence). As shown by the fluorescence intensity profile along the indicated dotted lines, treatment with VTP reduced the co-localization of αSMA and F-Actin signals (indicated by * in each of the plots corresponding) that was elevated by treatment with TGF-β1. **C**, Reduction of αSMA protein expression and of collagen-1 secretion by VTP treatment. The top left panel indicates the integration of the αSMA IF signal calculated as the integrated fluorescence density using ImageJ software. The panel on the top right represents an example of a Western blotting analysis performed with whole protein extracts from cSt-Cs treated as indicated. Note the decrease of the αSMA band intensity in VTP-treated cells compared with controls and TGF-β1 treatment, also indicated in the bar graph in the low right, showing quantification of the normalized αSMA/GAPDH in all the conditions. The panel on the low left indicates the reduction in collagen secretion by the cells treated with VTP vs CTRL and TGF-β1 treatment. Also in this case, this reduction occurred also in the combined VTP+TGF-β1 treatment. Above all graphs, the *P* indicate the results of data statistical comparison by 1-way pairwise ANOVA with Tukey post hoc test. **D**, The ability of the cells to remodel the matrix was assessed by the collagen plug contraction assay. The panels on the top show the top-view images of the plugs containing cells treated as indicated, while the bar graph on the bottom shows the quantification of the area occupied by the plug at 24 hours after matrix release. Lower areas are indicative of a higher contraction activity, in response to Myo-Fb differentiation of human cSt-Cs determined by TGF-β1. VTP treatment completely reverted the contractile phenotype of the cSt-Cs. Above the graphs, the *P* indicate the results of data statistical comparison by 1-way pairwise ANOVA with Tukey post hoc test. **F**, Untreated and TGF-β1-treated cSt-Cs±VTP were seeded onto PDMS micropillars to calculate the average traction force. The picture on the top illustrates the phase contrast image of a cell deposited onto the pillar array (left) and its corresponding F-Actin (red)/nuclear (blue) staining. The picture on the bottom is a virtual representation of the traction forces exerted by the cell onto each individual pillar, its direction (arrows) and intensity (color code). The graph on the bottom represents the average force exerted by a total of 12 cells (3 cells per donor) in the four treatment conditions.

the 3D gel containing cSt-Cs treated with TGF-β1, as opposed to control cells, and cells treated with TGF-β1+VTP. Interestingly, cell force analysis by measuring the bending of PDMS micropillars did not show differences between the average forces developed by the cells treated under the different conditions (Figure 6E). Together, these results show that interfering with YAP-dependent transcriptional activity blocks differentiation of cSt-Cs into myofibroblasts induced by TGF-β1 and limits their matrix remodeling and compacting ability, without affecting the physiological intracellular transmission of mechanical forces.

Antifibrotic Activity of VTP in a Mouse Model of Ischemic Cardiac Fibrosis

To verify the possible anti-fibrotic activity of VTP in vivo, we set a mouse model of ischemic cardiac remodeling

in mice. The treatment protocol of mice was in line with existing literature on the anti-fibrotic effects of VTP in other organs, such as kidney.[58] Two time-points were chosen to assess the effects of the continuous drug administration in relationships with the known biphasic myocardial remodeling process characterized by a precocious inflammatory phase (7 days), followed by an anti-inflammatory phase characterized by scar formation and collagen deposition (day 28). The experiment was controlled by evaluating the cardiac function by echocardiography and, finally by histological examination of the explanted heart at 7 and 28 days. The results of this experiment are summarized in Figure 7, where it is clearly shown that administration of VTP reduced the extent of the fibrotic areas at either 7 or 28 days post-MI (Figure 7A through 7D). It was interesting to note that the fibrotic areas in VTP-treated mice were less compact (compare insets in Figure 7C versus those in Figure 7D) and, in some cases, exhibited a higher number of CMs resembling the interstitial fibrosis detected in patients with ischemic cardiomyopathy (Figure 1). The anti-fibrotic effect of VTP also determined a significant increase in infarct thickness and a reduction of the infarct size at 7 and to a lesser extent at day 28 (Figure 7D). The positive effect on fibrosis of VTP was not, however, counterbalanced by an improvement in cardiac function, as shown by the failure of the treatment to increase ejection fraction and left ventricle fractional shortening as well as to decrease the end-diastolic/systolic volumes (Figure 7E).

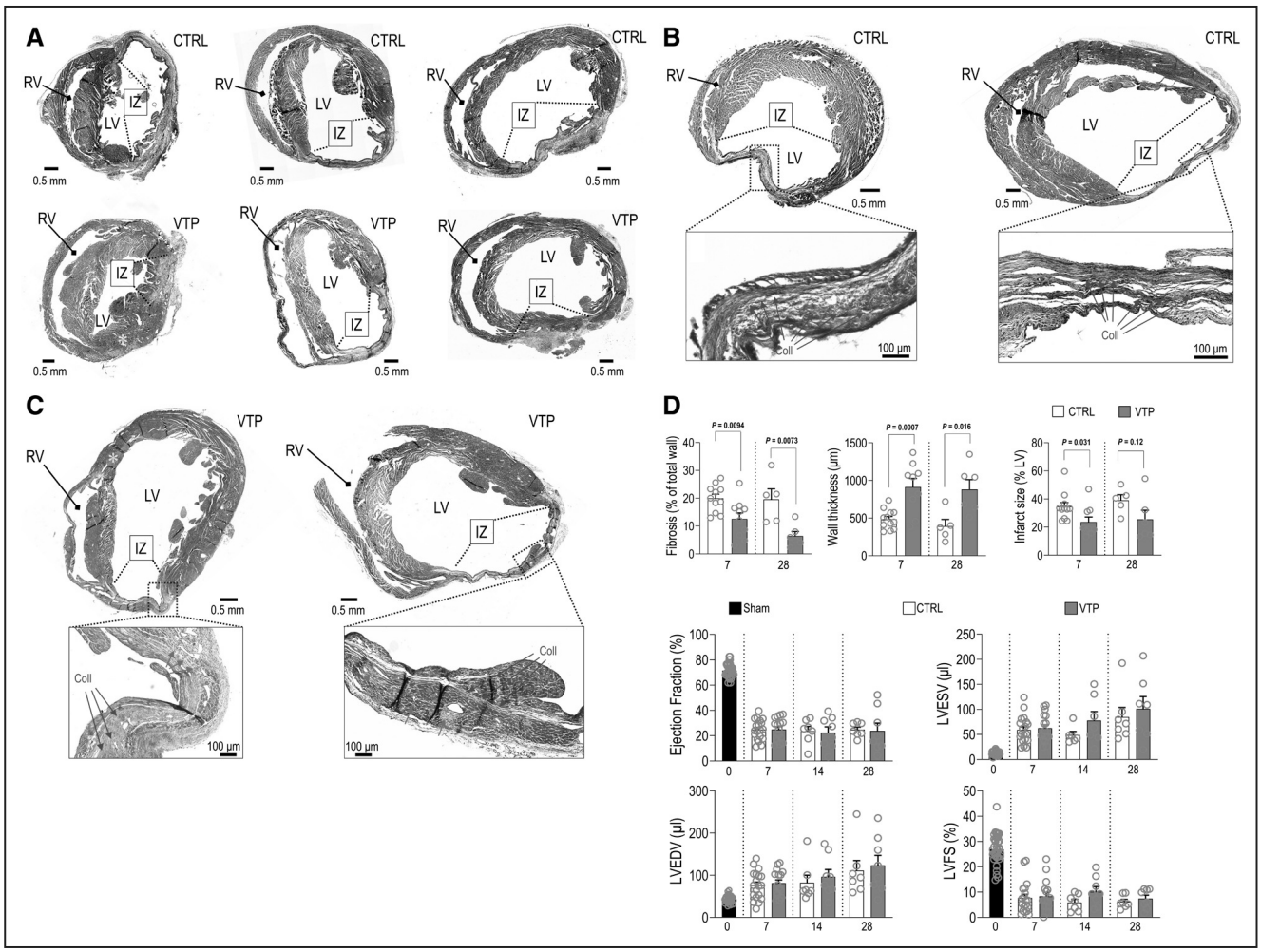

Figure 7. Effects of VTP (verteporfin) treatment on cardiac fibrosis and function in a mouse model of permanent cardiac ischemia. **A**, Side by side comparison of equatorial sections of infarcted hearts harvested at 7 days post-myocardial infarction (MI) from control (CTRL) and VTP-treated mice after staining with Masson's trichrome. It is evident the higher extension of the infarct, the higher collagen deposition, and the thinning of the scar in CTRL vs VTP mice. **B** and **C**, Side by side comparison of the scars at 28 days after MI in CTRL and VTP-treated mice. Also at this time point VTP reduced fibrosis and increased thickness of the infarct. Less evident was the effect of the drug on reduction of the infarct size. **D**, Quantification of the infarct morphometry as detected in the tissue sections stained with Masson's trichrome at 7 and 28 days after MI. VTP reduced significantly the fibrosis and the infarct size and increased the wall thickness indicative of a lower LV remodeling. This effect was more pronounced at 7 days given that the reduction of the infarct size at 28 days post-MI did not reach statistical significance. Above all graphs, the *P* indicate the results of data statistical comparison by pairwise Student *t* test. **E**, None of the echocardiographic parameters (ejection fraction, LV end diastolic/systolic volumes, and fractional shortening) were affected by the treatment at neither time.

DISCUSSION

Relevance of Extracellular Matrix Remodeling for Activation of YAP-Pathway In Vivo

Previous investigations highlighted the importance of the YAP signaling in cardiac fibrosis. For example, it was found that cells in the infarct zone in mice exhibit YAP nuclear staining[25] and that in mice lacking Lats1/2 kinases, two components of the Hippo kinase pathway, cardiac fibroblasts transition into Myo-Fbs spontaneously, giving rise to a hyper-secretory phenotype worsening the outcome of MI.[24]

Since Lats proteins phosphorylate directly YAP preventing its nuclear translocation,[56] the authors investigated the promoter occupancy of the chromatin in wt and Lats$^{-/-}$ CFs and found significant enrichment of YAP-bound enhancer sites in profibrotic genes in knockout cells. This evidence led them to conclude that YAP/TAZ complex promotes cardiac fibroblasts transitioning into myo-Fbs by stable modifications of chromatin architecture and activity. In keeping with these conclusions, selective genetic ablation of YAP in cardiac fibroblasts, reduced cardiac fibrosis and improved cardiac function after MI.[26,59]

To assess whether the active matrix remodeling creates permissive conditions for YAP nuclear translocation in cells with morphological characteristics of Myo-Fbs, we employed a mouse model of MI and characterized the features of the cells exhibiting nuclear YAP localization as a criterion to determine its transcriptional activity in vivo.[25,56] In this analysis, we took as a reference evidences emerging from computational models describing the regional deposition of collagen fibers following myocardial injury, where nonrandom patterns have been observed, likely depending on the alignment of the cells depositing the matrix caused by the anisotropic distribution of the strain forces.[37] Strikingly, as revealed by the nuclear ellipticity and orientation analyses performed in cells with the morphology of CFs in the scars at 4 weeks post-MI (Figure 1), we noticed a more frequent occurrence of nuclei with a more elongated shape and a more consistent alignment along the equatorial cutting plane of the left ventricle in cells with nuclear-localized YAP. Since the orientation of the nuclei in the infarct and, more in general, inside 3D matrices subjected to strain with a principally uniaxial component aligns the cells and the ECM deposition along the principal force vector,[60] the prevalent nuclear translocation of YAP in cells with a higher nuclear ellipticity and a more frequent cellular circumferential orientation might be part of a strain-dependent anisotropic activation of the *pro*-healing response to infarct reinforcing the cardiac wall and preventing its immediate rupture after infarction, but promoting chronic ventricular remodeling (hypothetical model described in Figure 8).[61] This hypothesis is corroborated by results showing that matrix remodeling in the infarcted heart involves a complex series of structural modifications, changes in mechanical properties and hyperactivation of profibrotic signaling,[62] as well as by evidences in other tissues, for example, the cardiac valves, where the deformation of the nuclei in interstitial cells has been connected to cyclic deformations due to straightening and compaction of the fibrous ECM components (ie, collagen).[63] This validates YAP as a transcriptional sensor of the dynamic remodeling of the cardiac ECM consequent to ischemic damage. Its expression in nuclei of CFs in the fibrotic areas in myocardial samples of patients with severe heart failure (Figure 1) suggests the possible activity of the pathway in the human pathology.

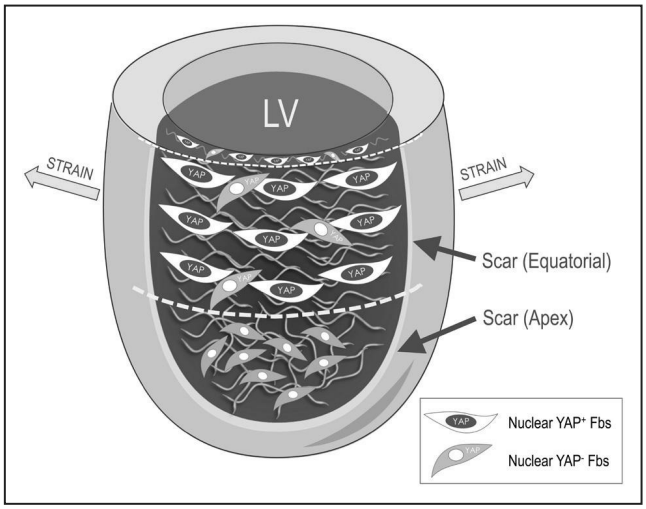

Figure 8. Proposed model of strain-dependent YAP (yes-associated protein) transcriptional signaling activation in the infarct scar.
Myocardial remodeling after a transmural infarction involves matrix deposition and this occurs, according to literature, with a preferential equatorial orientation. This deposition pattern is due to a strain-dependent alignment of the collagen depositing cells along the principal strain vector. The findings in this work show that the variation in the nuclear aspect ratio in the collagen-depositing cells is connected to nuclear translocation of YAP. We propose that this creates a permanent activation condition of these cells toward a profibrotic phenotype. Given that existing models of anisotropic collagen deposition in injured hearts describe this phenomenon only for regions of the cardiac wall at a distance from the LV apex,[37] we cautiously extend our hypothetical model only to regions of the cardiac wall, where the distribution of strain forces occurs principally with an equatorial direction, and not in the apex. Further studies involving in vivo cardiac kinematics and serial sectioning of the scars at different sectioning planes would be necessary to further validate this hypothesis for the whole ventricular wall.

Cell/Nuclear Strain/Compression-Dependence of a Profibrotic Pathway in Human Cardiac Stromal Cells

Human primitive cardiac stromal cells have been shown to display profibrotic features when exposed to the native extracellular matrix from remodeled hearts, or even to

the altered substrates synthesized ex vivo by pathological cardiac fibroblasts from failing hearts.[62,64,65] To get insights in the mechanically activated profibrotic evolution of the primitive human stromal cells, we employed a 2D cell culture system to test the effects of discrete cytoskeleton tensioning on the activation of YAP target genes, and to assess reversion of the profibrotic phenotype by treating cells with inhibitors of the F-Actin cytoskeleton. In line with evidences provided in other studies, performed either on cardiac or valve stromal cells,[29,43,52,66] human cSt-Cs exhibited a stiffness-dependent YAP nuclear translocation resulting into cell proliferation (Figure 2). When treated with inhibitors of the cytoskeleton tensioning, cSt-Cs reversibly extruded YAP from the nucleus and downregulated canonical transcriptional targets and profibrotic genes (Figure 4). It was finally interesting to note that nucleus geometry and compliance were also reversibly affected by the release of cytoskeleton tensioning by the 2 inhibitors (Figure 3). The change in nuclear geometry due to relaxation along the *z*-axis of the microscopic view likely reflects the release of the nuclear tensioning—acting mainly in the 2D (*x*, *y*) dimensions—due to adherence of the cells to a rigid flat surface,[17] similarly to the effect of plating the cells onto soft substrates (Figure 2). The decrease in nuclear compliance suggests a possible effect of releasing cytoskeleton tensioning not only on the reduction of the strain at the level of the nuclear lamina, but also on generalized changes in the chromatin compaction possibly leading to modifications in the epigenetic setup. In line with these evidences, it was demonstrated that biophysical cues can alter the methylation and acetylation status of histones, favoring epithelial to mesenchymal transition,[67] and that cells embedded into matrices simulating stiff pathological tissues exhibit a mechanical memory establishing permanent activation of pathological programs.[68] Whether, and to what extent, the nuclear straining imposed by cytoskeleton tensioning in human cSt-Cs has an epigenetic readout is the subject of ongoing investigations.

The connection between YAP nuclear translocation, nuclear straining and activation of profibrotic signaling was optimally validated in cardiospheres. Apart from the description of this model as an in vitro 'niche' of cardiac mesenchymal progenitors,[39] the cardiosphere appeared to fulfill the characteristics of a suitable 3D system to assess the impact of cell/nuclear straining on YAP-dependent profibrotic activation in cSt-Cs, in analogy to what we observed in the fibrotic scar in mice (Figure 1). We adopted this model by extending concepts validated in the earliest stages of mammalian embryogenesis, where mechanical-dependent inhibition of the Hippo pathway and a robust YAP nuclear translocation have been described as a topological determinant of the primitive trophectoderm cells differentiation in the cellular shell of the forming blastocyst.[69] To validate this model, we computer-analyzed the deformation of the nuclei in the cellular spheroids in relationship with the position of the cells in the core versus the shell of the cardiospheres, the presence of nuclear-localized YAP, the expression of cell proliferation and profibrotic cellular markers, and the deposition of ECM components (Figure 3). The suitability of this method, based on the CARE algorithm,[34] allowed to establish rapidly, and with a high level of significance, a cause-effect relationship between the extent of nuclear deformation, the YAP nuclear translocation and the presence of Myo-Fb features (such as proliferation, expression of αSMA and collagen) in the cells depending on their 3D positioning, with cells in the shell characterized by higher strain versus those positioned in the core subjected to lower compression forces and strain. These evidences support, finally, the in vivo findings showing the effects of topological cues on the activity of the YAP signaling in a 3D multicellular cardiac fibrotic context (Figure 1).

Targeting Downstream Effectors of Mechanical Cues Reverts TGF-β-Dependent and Independent Cardiac Fibroblast Fibrotic Programming

The data of our RNAseq analysis support the notion that treating cells with VTP disassembles the bridging of YAP to TEADs regardless of cell strain and has unbalancing effects for the activity of the Hippo pathway with possible readouts on the level of YAP phosphorylation, transcriptional cooperation with the Wnt pathway, *YAP1* gene silencing (Figure 5B and 5C) and downregulation of several pathways connected with extracellular matrix remodeling, inflammation and cell polarity/migration (Figure S9A). Interestingly, cells treated with VTP also downregulated more than a half of the genes that were induced by TGF-β1, one of the most potent cardiac fibrosis-inducing factors[50,62] (Figure S8). These genes included canonical YAP targets such as *CTGF (CCN2)* and *ACTA2*, genes connected to the CFs profibrotic phenotype (*Thy-1*), and genes encoding for major scar components such as *COLA1* and *COLA3*. The centrality of the YAP/TAZ transcriptional signaling in the context of fibrotic activation of human cSt-Cs emerged, finally, from the bioinformatics search of the *cis*-regulatory elements potentially involved in the generalized gene downregulation observed in VTP-treated cells (±TGF-β1) versus controls (Figure S9B). This search identified TEAD 1/3/4 and the common transcriptional transducer of TGF-β signaling SMAD4 as candidates for the co-regulation of genes involving YAP/TAZ complex as a common factor. While this is in line with the current literature identifying cooperation of these transcriptional modulators,[70] it also highlights the centrality of the YAP/TAZ complex in the context of the TGF-β1 transcriptional signaling,[71] suggesting effectiveness of mechano-therapeutic approaches to reduce the extent of fibrosis in the

cardiovascular system and other organs controlled by the profibrotic factor.

In agreement with the variation in gene expression signatures, the blockade of YAP/TAZ/TEAD interaction by VTP also appeared to completely override the TGF-β1-dependent profibrotic activation of cSt-Cs on a phenotypic and functional points of view. This was substantiated by the reduction in cell proliferation (Figure 6C), the unloading of SMA from the F-Actin cytoskeleton (Figure 6B), and the inhibition of collagen secretion/matrix compaction ability of the cells treated with TGF-β1 (Figure 6C and 6D). Opposite to our hypothesis that cells treated with TGF-β1 might increase pulling forces, the experiment on micropillar arrays did not show any variation in cell contractility (Figure 6E). This finding is only in apparent contradiction with the reduction in matrix compaction due to VTP treatment, considering that other factors such as secretion of matrix remodeling enzymes may concur to the increased collagen compaction of the cells treated with TGF-β1.

Antifibrotic Effect of VTP Treatment In Vivo Does Not Coincide With Improvement of Cardiac Function

The interest for manipulating the Hippo pathway as a strategy to repair/regenerate the heart has produced a growing course of studies with remarkable, but sometimes antagonistic results (reviewed in study by Meng et al[72]). In fact, the existing literature clearly distinguishes between the function of the YAP/TAZ complex in the heart, depending on the localization of the loss/gain of function effects. For example, while upregulation/stabilization of YAP in CMs primes the contractile cells to divide, with potential cardiac regenerating effects,[19,20,22] the hyperactivation of the YAP/TAZ complex in cardiac fibroblasts primes these cells toward a chronic scarring phenotype that result in accelerated and injury-independent myocardial remodeling[24] (also discussed in study by Johansen and Molkentin[23]). On the other hand, more recent studies showed that selective ablation of YAP in CFs reduces ischemia or pressure overload-dependent fibrosis with an improvement of myocardial function,[26,59] thus opening the way to possible mechano-therapeutic strategies to limit cardiac fibrosis.

Prompted by the positive effects of VTP administration in models of ischemia/reperfusion-dependent kidney fibrosis,[58] in the present study, we used a classical VTP continuous administration protocol in mice with a chronic cardiac ischemia setting. Although this clearly reduced the accumulation of collagen and, at least in part, preserved the infarct wall from the extreme thinning observed in control mice, the administration of the drug did not relief the detrimental effects of ischemia on cardiac function (Figure 7). Different possibilities may account for this effect, which makes the results of our findings clearly different from those achieved in genetic models of selective YAP inhibition in CFs. A first element that may play a role in this difference is the possibility that VTP alters/retards the timing of the pro/anti-inflammatory phases after cardiac damage. For example, Freeman et al[36] showed that selective ablation of YAP in early stage macrophages after MI promoted cardiac repair by shifting the phenotype of these cells toward an anti-inflammatory phenotype. In line with this, our treatment with VTP could have an initially positive effect on selective ablation of pro-inflammatory macrophages but, thereafter, a pleiotropic inhibiting function of anti-inflammatory macrophages with detrimental effects for cardiac functional recovery. A second possibility may derive from the ambivalent function of the YAP/TAZ complex in cardiac myocytes versus fibroblasts. For example, YAP loss of function in CMs leads to impaired survival after cardiac injury with worsening effects on maladaptive ventricular remodeling after myocardial injury.[73] In such a case, the beneficial effect of VTP administration on reduction of fibrosis might be counteracted by a reduced survival of myocytes in the infarcted heart, thus limiting the therapeutic efficacy of bulk administration of the drug. To substantiate our results in translational and functional perspectives, we are currently evaluating, (1) other treatment modalities (eg, to start or interrupt administration of the drug at defined times after the initial pro-inflammatory period) to better distinguish between possible antagonistic effects of the continuous VTP treatment on myocardial functional recovery, (2) the adoption of imaging-derived parameters of global cardiac function such as the myocardial strain,[74] (3) the use of 3D imaging tools such as the second harmonic generation microscopy,[62] and (4) of force-based mapping by nanoindentation[29] of the cardiac tissue.

CONCLUSIONS

The emerging role of YAP in fibrotic progression in several diseases,[75] including myocardial remodeling after infarction,[25] provides a strong rationale for a potential anti-fibrotic therapy of the failing heart, based on local mechanical desensitization of the profibrotic cells. Translation of genetic approaches into protocols of selective pharmacological inhibition of the complex in CFs but not in CMs is, in fact, not currently amenable using systemic administration protocols.

In the present study, we provide evidences that the profibrotic programming of human cSt-Cs in vitro is subjected to the cooperation of mechanical, topological and paracrine cues likely originating from the known effects of strain forces resulting from the anisotropic arrangement of the collagen matrix occurring during scar formation[37,76] (Figure 8), and the results of the nuclear strain/orientation analyses performed on YAP^{+} and YAP^{-} nuclei in the infarct fibrotic scar. We extend this conclusion also to an in vivo cardiac remodeling situation, where the administration of VTP caused a significant inhibition of the fibrotic progression in the ischemic hearts, although this improvement was not accompanied by a net increase in cardiac performance.

A final and more general conclusion of our investigation is that, in analogy to what already described in other cardiovascular pathological settings such as the aortic valve disease[29,77] or vascular pathological conditions,[78,79] understanding the cooperation between mechanical cues and paracrine factors in cardiovascular diseases will be a possible key to achieve innovative and targeted antifibrotic therapies. Indeed, if administered with systems specifically designed to perform drug delivery in the fibrotic tissues (eg, nanotechnology), these therapies will be optimal candidates to mechanically desensitize the profibrotic cells, with hopes for robust reverse remodeling effects.

ARTICLE INFORMATION

Received April, 15 2021; revision received May 25, 2022; accepted June 13, 2022

Affiliations

Centro Cardiologico Monzino, IRCCS, Milan, Italy (G.G., M.C., F.A., G.B., L.P., E.Z., S.R., M.C., S.F., R.S., M.M., A.R., G.I.C., M.P.). Department of Mechanical and Aerospace Engineering, Politecnico di Torino, Turin, Italy (M.S., D.C., F. Molinari, D.M., U.M.). Department of Medical Surgical Science and Biotechnology, Sapienza University of Rome (I.C., C.C.). Mediterranea Cardiocentro, Napoli (I.C.). Policlinico San Donato, IRCCS (G.Z., L.M., F. Martelli). Elettra Sincrotrone ScPA, Trieste, Italy (G.M., L.C.). Dipartimento di Scienze Biomediche, Chirurgiche ed Odontoiatriche, Università di Milano, Milan, Italy (M.A.). Faculty of Engineering, Hokkaido University, Sapporo, Japan (O.B., T.O.). Institute of Biochemistry and Cell Biology, National Council of Research (IBBC-CNR), Monterotondo, Italy (F.P.). Department of Pediatrics and Infant Neuropsychiatry. Policlinico Umberto I, Sapienza University of Rome (E.M.).

Sources of Funding

The present research was funded by the Institutional research funding by Italian Ministry of Health (Ricerca Corrente; Ricerca 5 per mille) granted to M. Pesce, G. Zaccagnini, L. Menicanti, and FM; by the European Union MEDIRAD project granted to I. Chimenti and E. Messina, who received funding from the Euratom research and training programme 2014 to 2018 under grant agreement No. 755523; by RG11916B85CDBF76 granted from Sapienza University to I. Chimenti; by Ricerca Finalizzata RF-12368521 to F. Martelli. F. Martelli is also supported by Telethon-Italy (No. GGP19035), AFM-Téléthon (No. 23054), the EU Horizon 2020 project COVIRNA (Grant No. 101016072), and the EU-CardioRNA COST Action CA17129.

Disclosures

None.

Supplemental Material

Expanded Materials and Methods
Figures S1–S9
References 80–99
Major Resource Table
Uncut Gel Blots

REFERENCES

1. de Boer RA, De Keulenaer G, Bauersachs J, Brutsaert D, Cleland JG, Diez J, Du XJ, Ford P, Heinzel FR, Lipson KE, et al. Towards better definition, quantification and treatment of fibrosis in heart failure. A scientific roadmap by the Committee of Translational Research of the Heart Failure Association (HFA) of the European Society of Cardiology. *Eur J Heart Fail*. 2019;21:272–285. doi: 10.1002/ejhf.1406
2. Ruiz-Villalba A, Romero JP, Hernández SC, Vilas-Zornoza A, Fortelny N, Castro-Labrador L, San Martin-Uriz P, Lorenzo-Vivas E, García-Olloqui P, Palacio M, et al. Single-cell RNA sequencing analysis reveals a crucial role for CTHRC1 (Collagen Triple Helix Repeat Containing 1) cardiac fibroblasts after myocardial infarction. *Circulation*. 2020;142:1831–1847. doi: 10.1161/CIRCULATIONAHA.119.044557
3. Farbehi N, Patrick R, Dorison A, Xaymardan M, Janbandhu V, Wystub-Lis K, Ho JW, Nordon RE, Harvey RP. Single-cell expression profiling reveals dynamic flux of cardiac stromal, vascular and immune cells in health and injury. *Elife*. 2019;8:e43882. doi: 10.7554/eLife.43882
4. Forte E, Furtado MB, Rosenthal N. The interstitium in cardiac repair: role of the immune-stromal cell interplay. *Nat Rev Cardiol*. 2018;15:601–616. doi: 10.1038/s41569-018-0077-x
5. Schroer AK, Merryman WD. Mechanobiology of myofibroblast adhesion in fibrotic cardiac disease. *J Cell Sci*. 2015;128:1865–1875. doi: 10.1242/jcs.162891
6. Tallquist MD, Molkentin JD. Redefining the identity of cardiac fibroblasts. *Nat Rev Cardiol*. 2017;14:484–491. doi: 10.1038/nrcardio.2017.57
7. van Putten S, Shafieyan Y, Hinz B. Mechanical control of cardiac myofibroblasts. *J Mol Cell Cardiol*. 2016;93:133–142. doi: 10.1016/j.yjmcc.2015.11.025
8. Souders CA, Bowers SL, Baudino TA. Cardiac fibroblast: the renaissance cell. *Circ Res*. 2009;105:1164–1176. doi: 10.1161/CIRCRESAHA.109.209809
9. Porter KE, Turner NA. Cardiac fibroblasts: at the heart of myocardial remodeling. *Pharmacol Ther*. 2009;123:255–278. doi: 10.1016/j.pharmthera.2009.05.002
10. Horn MA. Cardiac physiology of aging: extracellular considerations. *Compr Physiol*. 2015;5:1069–1121. doi: 10.1002/cphy.c140063
11. Pesce M, Santoro R. Feeling the right force: How to contextualize the cell mechanical behavior in physiologic turnover and pathologic evolution of the cardiovascular system. *Pharmacol Ther*. 2017;171:75–82. doi: 10.1016/j.pharmthera.2016.08.002
12. Zanconato F, Cordenonsi M, Piccolo S. YAP/TAZ at the roots of cancer. *Cancer Cell*. 2016;29:783–803. doi: 10.1016/j.ccell.2016.05.005
13. Brusatin G, Panciera T, Gandin A, Citron A, Piccolo S. Biomaterials and engineered microenvironments to control YAP/TAZ-dependent cell behaviour. *Nat Mater*. 2018;17:1063–1075. doi: 10.1038/s41563-018-0180-8
14. Panciera T, Azzolin L, Cordenonsi M, Piccolo S. Mechanobiology of YAP and TAZ in physiology and disease. *Nat Rev Mol Cell Biol*. 2017;18:758–770. doi: 10.1038/nrm.2017.87
15. Aragona M, Panciera T, Manfrin A, Giulitti S, Michielin F, Elvassore N, Dupont S, Piccolo S. A mechanical checkpoint controls multicellular growth through YAP/TAZ regulation by actin-processing factors. *Cell*. 2013;154:1047–1059. doi: 10.1016/j.cell.2013.07.042
16. Dupont S, Morsut L, Aragona M, Enzo E, Giulitti S, Cordenonsi M, Zanconato F, Le Digabel J, Forcato M, Bicciato S, et al. Role of YAP/TAZ in mechanotransduction. *Nature*. 2011;474:179–183. doi: 10.1038/nature10137
17. Elosegui-Artola A, Andreu I, Beedle AEM, Lezamiz A, Uroz M, Kosmalska AJ, Oria R, Kechagia JZ, Rico-Lastres P, Le Roux AL, et al. Force triggers YAP nuclear entry by regulating transport across nuclear pores. *Cell*. 2017;171:1397–1410.e14. doi: 10.1016/j.cell.2017.10.008
18. Pesce M, Messina E, Chimenti I, Beltrami AP. Cardiac mechanoperception: a life-long story from early beats to aging and failure. *Stem Cells Dev*. 2017;26:77–90. doi: 10.1089/scd.2016.0206
19. Monroe TO, Hill MC, Morikawa Y, Leach JP, Heallen T, Cao S, Krijger PHL, de Laat W, Wehrens XHT, Rodney GG, et al. YAP partially reprograms chromatin accessibility to directly induce adult cardiogenesis in vivo. *Dev Cell*. 2019;48:765–779.e7. doi: 10.1016/j.devcel.2019.01.017
20. Xin M, Kim Y, Sutherland LB, Murakami M, Qi X, McAnally J, Porrello ER, Mahmoud AI, Tan W, Shelton JM, et al. Hippo pathway effector Yap promotes cardiac regeneration. *Proc Natl Acad Sci U S A*. 2013;110:13839–13844. doi: 10.1073/pnas.1313192110
21. Morikawa Y, Heallen T, Leach J, Xiao Y, Martin JF. Dystrophin-glycoprotein complex sequesters Yap to inhibit cardiomyocyte proliferation. *Nature*. 2017;547:227–231. doi: 10.1038/nature22979
22. Leach JP, Heallen T, Zhang M, Rahmani M, Morikawa Y, Hill MC, Segura A, Willerson JT, Martin JF. Hippo pathway deficiency reverses systolic heart failure after infarction. *Nature*. 2017;550:260–264. doi: 10.1038/nature24045
23. Johansen AKZ, Molkentin JD. Hippo signaling does it again: arbitrating cardiac fibroblast identity and activation. *Genes Dev*. 2019;33:1457–1459. doi: 10.1101/gad.332791.119
24. Xiao Y, Hill MC, Li L, Deshmukh V, Martin TJ, Wang J, Martin JF. Hippo pathway deletion in adult resting cardiac fibroblasts initiates a cell state transition with spontaneous and self-sustaining fibrosis. *Genes Dev*. 2019;33:1491–1505. doi: 10.1101/gad.329763.119

25. Mosqueira D, Pagliari S, Uto K, Ebara M, Romanazzo S, Escobedo-Lucea C, Nakanishi J, Taniguchi A, Franzese O, Di Nardo P, et al. Hippo pathway effectors control cardiac progenitor cell fate by acting as dynamic sensors of substrate mechanics and nanostructure. *ACS Nano*. 2014;8:2033–2047. doi: 10.1021/nn4058984
26. Francisco J, Zhang Y, Jeong JI, Mizushima W, Ikeda S, Ivessa A, Oka S, Zhai P, Tallquist MD, Del Re DP. Blockade of fibroblast YAP attenuates cardiac fibrosis and dysfunction through MRTF-A inhibition. *JACC Basic Transl Sci*. 2020;5:931–945. doi: 10.1016/j.jacbts.2020.07.009
27. Feng J, Gou J, Jia J, Yi T, Cui T, Li Z. Verteporfin, a suppressor of YAP-TEAD complex, presents promising antitumor properties on ovarian cancer. *Onco Targets Ther*. 2016;9:5371–5381. doi: 10.2147/OTT.S109979
28. Goumans MJ, Ten Dijke P. Tgf-beta signaling in control of cardiovascular function. *Cold Spring Harbor Perspect Biol*. 2018;10:a031989. doi: 10.1101/cshperspect.a031989
29. Santoro R, Scaini D, Severino LU, Amadeo F, Ferrari S, Bernava G, Garoffolo G, Agrifoglio M, Casalis L, Pesce M. Activation of human aortic valve interstitial cells by local stiffness involves YAP-dependent transcriptional signaling. *Biomaterials*. 2018;181:268–279. doi: 10.1016/j.biomaterials.2018.07.033
30. Tan JL, Tien J, Pirone DM, Gray DS, Bhadriraju K, Chen CS. Cells lying on a bed of microneedles: an approach to isolate mechanical force. *Proc Natl Acad Sci U S A*. 2003;100:1484–1489. doi: 10.1073/pnas.0235407100
31. du Roure O, Saez A, Buguin A, Austin RH, Chavrier P, Silberzan P, Siberzan P, Ladoux B. Force mapping in epithelial cell migration. *Proc Natl Acad Sci U S A*. 2005;102:2390–2395. doi: 10.1073/pnas.0408482102
32. Messina E, De Angelis L, Frati G, Morrone S, Chimenti S, Fiordaliso F, Salio M, Battaglia M, Latronico MV, Coletta M, et al. Isolation and expansion of adult cardiac stem cells from human and murine heart. *Circ Res*. 2004;95:911–921. doi: 10.1161/01.RES.0000147315.71699.51
33. Chimenti I, Gaetani R, Forte E, Angelini F, De Falco E, Zoccai GB, Messina E, Frati G, Giacomello A. Serum and supplement optimization for EU GMP-compliance in cardiospheres cell culture. *J Cell Mol Med*. 2014;18:624–634. doi: 10.1111/jcmm.12210
34. Salvi M, Morbiducci U, Amadeo F, Santoro R, Angelini F, Chimenti I, Massai D, Messina E, Giacomello A, Pesce M, et al. Automated segmentation of fluorescence microscopy images for 3d cell detection in human-derived cardiospheres. *Sci Rep*. 2019;9:6644. doi: 10.1038/s41598-019-43137-2
35. Di Maggio S, Milano G, De Marchis F, D'Ambrosio A, Bertolotti M, Palacios BS, Badi I, Sommariva E, Pompilio G, Capogrossi MC, et al. Non-oxidizable HMGB1 induces cardiac fibroblasts migration via CXCR4 in a CXCL12-independent manner and worsens tissue remodeling after myocardial infarction. *Biochim Biophys Acta Mol Basis Dis*. 2017;1863:2693–2704. doi: 10.1016/j.bbadis.2017.07.012
36. Freeman TC, Mia MM, Cibi DM, Abdul Ghani SAB, Song W, Tee N, Ghosh S, Mao J, Olson EN, Singh MK. Yap/taz deficiency reprograms macrophage phenotype and improves infarct healing and cardiac function after myocardial infarction. *PLOS Biol*. 2020;18:e3000941. doi: 10.1371/journal.pbio.3000941
37. Fomovsky GM, Rouillard AD, Holmes JW. Regional mechanics determine collagen fiber structure in healing myocardial infarcts. *J Mol Cell Cardiol*. 2012;52:1083–1090. doi: 10.1016/j.yjmcc.2012.02.012
38. Chimenti I, Massai D, Morbiducci U, Beltrami AP, Pesce M, Messina E. Stem cell spheroids and ex vivo niche modeling: rationalization and scaling-up. *J Cardiovasc Transl Res*. 2017:1–17. doi: 10.1007/s12265-017-9741-5
39. Smith RR, Barile L, Cho HC, Leppo MK, Hare JM, Messina E, Giacomello A, Abraham MR, Marbán E. Regenerative potential of cardiosphere-derived cells expanded from percutaneous endomyocardial biopsy specimens. *Circulation*. 2007;115:896–908. doi: 10.1161/CIRCULATIONAHA.106.655209
40. Engler AJ, Sen S, Sweeney HL, Discher DE. Matrix elasticity directs stem cell lineage specification. *Cell*. 2006;126:677–689. doi: 10.1016/j.cell.2006.06.044
41. Barile L, Chimenti I, Gaetani R, Forte E, Miraldi F, Frati G, Messina E, Giacomello A. Cardiac stem cells: isolation, expansion and experimental use for myocardial regeneration. *Nat Clin Pract Cardiovasc Med*. 2007;4 Suppl 1:S9–S14. doi: 10.1038/ncpcardio0738
42. Forte E, Miraldi F, Chimenti I, Angelini F, Zeuner A, Giacomello A, Mercola M, Messina E. TGFβ-dependent epithelial-to-mesenchymal transition is required to generate cardiospheres from human adult heart biopsies. *Stem Cells Dev*. 2012;21:3081–3090. doi: 10.1089/scd.2012.0277
43. Ugolini GS, Rasponi M, Pavesi A, Santoro R, Kamm R, Fiore GB, Pesce M, Soncini M. On-chip assessment of human primary cardiac fibroblasts proliferative responses to uniaxial cyclic mechanical strain. *Biotechnol Bioeng*. 2016;113:859–869. doi: 10.1002/bit.25847
44. Peyton SR, Putnam AJ. Extracellular matrix rigidity governs smooth muscle cell motility in a biphasic fashion. *J Cell Physiol*. 2005;204:198–209. doi: 10.1002/jcp.20274
45. Bhadriraju K, Yang M, Alom Ruiz S, Pirone D, Tan J, Chen CS. Activation of ROCK by RhoA is regulated by cell adhesion, shape, and cytoskeletal tension. *Exp Cell Res*. 2007;313:3616–3623. doi: 10.1016/j.yexcr.2007.07.002
46. Szeto SG, Narimatsu M, Lu M, He X, Sidiqi AM, Tolosa MF, Chan L, De Freitas K, Bialik JF, Majumder S, et al. Yap/taz are mechanoregulators of tgf-β-smad signaling and renal fibrogenesis. *J Am Soc Nephrol*. 2016;27:3117–3128. doi: 10.1681/ASN.2015050499
47. Gibault F, Corvaisier M, Bailly F, Huet G, Melnyk P, Cotelle P. Non-photoinduced biological properties of verteporfin. *Curr Med Chem*. 2016;23:1171–1184. doi: 10.2174/0929867323666160316125048
48. Small EM, Brooks AC. Cut the yap limiting fibrosis in pathologic cardiac remodeling. *Jacc-Basic Transl Sc*. 2020;5:946–948. doi: 10.1016/j.jacbts.2020.08.004
49. Gago-Lopez N, Awaji O, Zhang Y, Ko C, Nsair A, Liem D, Stempien-Otero A, MacLellan WR. THY-1 receptor expression differentiates cardiosphere-derived cells with divergent cardiogenic differentiation potential. *Stem Cell Reports*. 2014;2:576–591. doi: 10.1016/j.stemcr.2014.03.003
50. Frangogiannis NG. Cardiac fibrosis. *Cardiovasc Res*. 2021;117:1450–1488. doi: 10.1093/cvr/cvaa324
51. Ramazani Y, Knops N, Elmonem MA, Nguyen TQ, Arcolino FO, van den Heuvel L, Levtchenko E, Kuypers D, Goldschmeding R. Connective tissue growth factor (CTGF) from basics to clinics. *Matrix Biol*. 2018;68-69:44–66. doi: 10.1016/j.matbio.2018.03.007
52. Niu L, Jia Y, Wu M, Liu H, Feng Y, Hu Y, Zhang X, Gao D, Xu F, Huang G. Matrix stiffness controls cardiac fibroblast activation through regulating YAP via AT1 R. *J Cell Physiol*. 2020;235:8345–8357. doi: 10.1002/jcp.29678
53. Lee Y, Kim NH, Cho ES, Yang JH, Cha YH, Kang HE, Yun JS, Cho SB, Lee SH, Paclikova P, et al. Dishevelled has a YAP nuclear export function in a tumor suppressor context-dependent manner. *Nat Commun*. 2018;9:2301. doi: 10.1038/s41467-018-04757-w
54. Strakova K, Matricon P, Yokota C, Arthofer E, Bernatik O, Rodriguez D, Arenas E, Carlsson J, Bryja V, Schulte G. The tyrosine Y2502.39 in Frizzled 4 defines a conserved motif important for structural integrity of the receptor and recruitment of disheveled. *Cell Signal*. 2017;38:85–96. doi: 10.1016/j.cellsig.2017.06.018
55. Mana-Capelli S, McCollum D. Angiomotins stimulate LATS kinase autophosphorylation and act as scaffolds that promote hippo signaling. *J Biol Chem*. 2018;293:18230–18241. doi: 10.1074/jbc.RA118.004187
56. Piccolo S, Dupont S, Cordenonsi M. The biology of YAP/TAZ: hippo signaling and beyond. *Physiol Rev*. 2014;94:1287–1312. doi: 10.1152/physrev.00005.2014
57. Riz I, Hawley RG. Increased expression of the tight junction protein TJP1/ZO-1 is associated with upregulation of TAZ-TEAD activity and an adult tissue stem cell signature in carfilzomib-resistant multiple myeloma cells and high-risk multiple myeloma patients. *Oncoscience*. 2017;4:79–94. doi: 10.18632/oncoscience.356
58. Zheng Z, Li C, Shao G, Li J, Xu K, Zhao Z, Zhang Z, Liu J, Wu H. Hippo-YAP/MCP-1 mediated tubular maladaptive repair promote inflammation in renal failed recovery after ischemic AKI. *Cell Death Dis*. 2021;12:754. doi: 10.1038/s41419-021-04041-8
59. Mia MM, Cibi DM, Binte Abdul Ghani SA, Singh A, Tee N, Sivakumar V, Bogireddi H, Cook SA, Mao J, Singh MK. Loss of yap/taz in cardiac fibroblasts attenuates adverse remodeling and improves cardiac function. *Cardiovasc Res*. 2021:118:1785–1804. doi: 10.1093/cvr/cvab205
60. D'Amore A, Nasello G, Luketich SK, Denisenko D, Jacobs DL, Hoff R, Gibson G, Bruno A, T Raimondi M, Wagner WR. Meso-scale topological cues influence extracellular matrix production in a large deformation, elastomeric scaffold model. *Soft Matter*. 2018;14:8483–8495. doi: 10.1039/c8sm01352g
61. Hung CL, Verma A, Uno H, Shin SH, Bourgoun M, Hassanein AH, McMurray JJ, Velazquez EJ, Kober L, Pfeffer MA, et al; VALIANT investigators. Longitudinal and circumferential strain rate, left ventricular remodeling, and prognosis after myocardial infarction. *J Am Coll Cardiol*. 2010;56:1812–1822. doi: 10.1016/j.jacc.2010.06.044
62. Perestrelo AR, Silva AC, Oliver-De La Cruz J, Martino F, Horváth V, Caluori G, Polanský O, Vinarský V, Azzato G, de Marco G, et al. Multiscale analysis of extracellular matrix remodeling in the failing heart. *Circ Res*. 2021;128:24–38. doi: 10.1161/CIRCRESAHA.120.317685

63. Huang HY, Liao J, Sacks MS. In-situ deformation of the aortic valve interstitial cell nucleus under diastolic loading. *J Biomech Eng*. 2007;129:880–889. doi: 10.1115/1.2801670
64. Belviso I, Angelini F, Di Meglio F, Picchio V, Sacco AM, Nocella C, Romano V, Nurzynska D, Frati G, Maiello C, et al. The microenvironment of decellularized extracellular matrix from heart failure myocardium alters the balance between angiogenic and fibrotic signals from stromal primitive cells. *Int J Mol Sci*. 2020;21:E7903. doi: 10.3390/ijms21217903
65. Pagano F, Angelini F, Castaldo C, Picchio V, Messina E, Sciarretta S, Maiello C, Biondi-Zoccai G, Frati G, Meglio FD, et al. Normal versus pathological cardiac fibroblast-derived extracellular matrix differentially modulates cardiosphere-derived cell paracrine properties and commitment. *Stem Cells Int*. 2017;2017:7396462. doi: 10.1155/2017/7396462
66. Ma H, Killaars AR, DelRio FW, Yang C, Anseth KS. Myofibroblastic activation of valvular interstitial cells is modulated by spatial variations in matrix elasticity and its organization. *Biomaterials*. 2017;131:131–144. doi: 10.1016/j.biomaterials.2017.03.040
67. Downing TL, Soto J, Morez C, Houssin T, Fritz A, Yuan F, Chu J, Patel S, Schaffer DV, Li S. Biophysical regulation of epigenetic state and cell reprogramming. *Nat Mater*. 2013;12:1154–1162. doi: 10.1038/nmat3777
68. Yang C, Tibbitt MW, Basta L, Anseth KS. Mechanical memory and dosing influence stem cell fate. *Nat Mater*. 2014;13:645–652. doi: 10.1038/nmat3889
69. Biggins JS, Royer C, Watanabe T, Srinivas S. Towards understanding the roles of position and geometry on cell fate decisions during preimplantation development. *Semin Cell Dev Biol*. 2015;47-48:74–79. doi: 10.1016/j.semcdb.2015.09.006
70. Piersma B, Bank RA, Boersema M. Signaling in fibrosis: TGF-β, WNT, and YAP/TAZ converge. *Front Med (Lausanne)*. 2015;2:59. doi: 10.3389/fmed.2015.00059
71. Hanna A, Humeres C, Frangogiannis NG. The role of Smad signaling cascades in cardiac fibrosis. *Cell Signal*. 2021;77:109826. doi: 10.1016/j.cellsig.2020.109826
72. Meng F, Xie B, Martin JF. Targeting the hippo pathway in heart repair. *Cardiovasc Res*. 2021:cvab291. doi: 10.1093/cvr/cvab291
73. Del Re DP, Yang Y, Nakano N, Cho J, Zhai P, Yamamoto T, Zhang N, Yabuta N, Nojima H, Pan D, et al. Yes-associated protein isoform 1 (Yap1) promotes cardiomyocyte survival and growth to protect against myocardial ischemic injury. *J Biol Chem*. 2013;288:3977–3988. doi: 10.1074/jbc.M112.436311
74. Amzulescu MS, De Craene M, Langet H, Pasquet A, Vancraeynest D, Pouleur AC, Vanoverschelde JL, Gerber BL. Myocardial strain imaging: review of general principles, validation, and sources of discrepancies. *Eur Heart J Cardiovasc Imaging*. 2019;20:605–619. doi: 10.1093/ehjci/jez041
75. Dey A, Varelas X, Guan KL. Targeting the hippo pathway in cancer, fibrosis, wound healing and regenerative medicine. *Nat Rev Drug Discov*. 2020;19:480–494. doi: 10.1038/s41573-020-0070-z
76. Rouillard AD, Holmes JW. Mechanical regulation of fibroblast migration and collagen remodelling in healing myocardial infarcts. *J Physiol*. 2012;590:4585–4602. doi: 10.1113/jphysiol.2012.229484
77. Mabry KM, Lawrence RL, Anseth KS. Dynamic stiffening of poly(ethylene glycol)-based hydrogels to direct valvular interstitial cell phenotype in a three-dimensional environment. *Biomaterials*. 2015;49:47–56. doi: 10.1016/j.biomaterials.2015.01.047
78. Garoffolo G, Ruiter MS, Piola M, Brioschi M, Thomas AC, Agrifoglio M, Polvani G, Coppadoro L, Zoli S, Saccu C, et al. Coronary artery mechanics induces human saphenous vein remodelling via recruitment of adventitial myofibroblast-like cells mediated by thrombospondin-1. *Theranostics*. 2020;10:2597–2611. doi: 10.7150/thno.40595
79. Groeneveld ME, Meekel JP, Rubinstein SM, Merkestein LR, Tangelder GJ, Wisselink W, Truijers M, Yeung KK. Systematic review of circulating, biomechanical, and genetic markers for the prediction of abdominal aortic aneurysm growth and rupture. *J Am Heart Assoc*. 2018;7:e007791. doi: 10.1161/JAHA.117.007791
80. Salvi M, Molinari F. Multi-tissue and multi-scale approach for nuclei segmentation in H&E stained images. *Biomed Eng Online*. 2018;17:89. doi: 10.1186/s12938-018-0518-0
81. Xu H, Lu C, Mandal M. An efficient technique for nuclei segmentation based on ellipse descriptor analysis and improved seed detection algorithm. *IEEE J Biomed Health Inform*. 2014;18:1729–1741. doi: 10.1109/JBHI.2013.2297030
82. Amendola A, Garoffolo G, Songia P, Nardacci R, Ferrari S, Bernava G, Canzano P, Myasoedova V, Colavita F, Castilletti C, et al. Human cardiosphere-derived stromal cells exposed to SARS-CoV-2 evolve into hyperinflammatory/pro-fibrotic phenotype and produce infective viral particles depending on the levels of ACE2 receptor expression. *Cardiovasc Res*. 2021;117:1557–1566. doi: 10.1093/cvr/cvab082
83. Gambini E, Pompilio G, Biondi A, Alamanni F, Capogrossi MC, Agrifoglio M, Pesce M. C-kit+ cardiac progenitors exhibit mesenchymal markers and preferential cardiovascular commitment. *Cardiovasc Res*. 2011;89:362–373. doi: 10.1093/cvr/cvq292
84. Ghibaudo M, Di Meglio JM, Hersen P, Ladoux B. Mechanics of cell spreading within 3D-micropatterned environments. *Lab Chip*. 2011;11:805–812. doi: 10.1039/c0lc00221f
85. Hermanowicz P, Sarna M, Burda K, Gabryś H. AtomicJ: an open source software for analysis of force curves. *Rev Sci Instrum*. 2014;85:063703. doi: 10.1063/1.4881683
86. Dobin A, Davis CA, Schlesinger F, Drenkow J, Zaleski C, Jha S, Batut P, Chaisson M, Gingeras TR. STAR: ultrafast universal RNA-seq aligner. *Bioinformatics (Oxford, England)*. 2013;29:15–21. doi: 10.1093/bioinformatics/bts635
87. Langmead B, Salzberg SL. Fast gapped-read alignment with bowtie 2. *Nat Methods*. 2012;9:357–359. doi: 10.1038/nmeth.1923
88. Liao Y, Smyth GK, Shi W. Featurecounts: an efficient general purpose program for assigning sequence reads to genomic features. *Bioinformatics (Oxford, England)*. 2014;30:923–930. doi: 10.1093/bioinformatics/btt656
89. Risso D, Schwartz K, Sherlock G, Dudoit S. GC-content normalization for RNA-Seq data. *BMC Bioinformatics*. 2011;12:480. doi: 10.1186/1471-2105-12-480
90. Chiesa M, Colombo GI, Piacentini L. DaMiRseq-an R/Bioconductor package for data mining of RNA-Seq data: normalization, feature selection and classification. *Bioinformatics*. 2018;34:1416–1418. doi: 10.1093/bioinformatics/btx795
91. Robinson MD, Oshlack A. A scaling normalization method for differential expression analysis of RNA-seq data. *Genome Biol*. 2010;11:R25. doi: 10.1186/gb-2010-11-3-r25
92. McCarthy DJ, Chen Y, Smyth GK. Differential expression analysis of multifactor RNA-Seq experiments with respect to biological variation. *Nucleic Acids Res*. 2012;40:4288–4297. doi: 10.1093/nar/gks042
93. Risso D, Ngai J, Speed TP, Dudoit S. Normalization of RNA-seq data using factor analysis of control genes or samples. *Nat Biotechnol*. 2014;32:896–902. doi: 10.1038/nbt.2931
94. Stevens JR, Herrick JS, Wolff RK, Slattery ML. Power in pairs: assessing the statistical value of paired samples in tests for differential expression. *BMC Genomics*. 2018;19:953. doi: 10.1186/s12864-018-5236-2
95. Leek JT, Storey JD. A general framework for multiple testing dependence. *Proc Natl Acad Sci U S A*. 2008;105:18718–18723. doi: 10.1073/pnas.0808709105
96. Ashburner M, Ball CA, Blake JA, Botstein D, Butler H, Cherry JM, Davis AP, Dolinski K, Dwight SS, Eppig JT, et al. Gene ontology: tool for the unification of biology. The gene ontology consortium. *Nat Genet*. 2000;25:25–29. doi: 10.1038/75556
97. Zhou Y, Zhou B, Pache L, Chang M, Khodabakhshi AH, Tanaseichuk O, Benner C, Chanda SK. Metascape provides a biologist-oriented resource for the analysis of systems-level datasets. *Nat Commun*. 2019;10:1523. doi: 10.1038/s41467-019-09234-6
98. Shannon P, Markiel A, Ozier O, Baliga NS, Wang JT, Ramage D, Amin N, Schwikowski B, Ideker T. Cytoscape: a software environment for integrated models of biomolecular interaction networks. *Genome Res*. 2003;13:2498–2504. doi: 10.1101/gr.1239303
99. Janky R, Verfaillie A, Imrichová H, Van de Sande B, Standaert L, Christiaens V, Hulselmans G, Herten K, Naval Sanchez M, Potier D, et al. Iregulon: from a gene list to a gene regulatory network using large motif and track collections. *PLoS Comput Biol*. 2014;10:e1003731. doi: 10.1371/journal.pcbi.1003731